Title

Computational Modeling of the Nature and Role of Ga Species for Light Alkane Dehydrogenation Catalyzed by Ga/H-MFI

Journal

ACS Catalysis, 8(7)

ISSN

2155-5435

Authors

Mansoor, E
Head-Gordon, M
Bell, AT

Publication Date

2018-07-06

DOI

10.1021/acscatal.7b04295

Peer reviewed

ACS Catalysis

Research Article

Cite This: ACS Catal. 2018, 8, 6146–6162

pubs.acs.org/acscatalysis

Computational Modeling of the Nature and Role of Ga Species for Light Alkane Dehydrogenation Catalyzed by Ga/H-MFI

Erum Mansoor,[†] Martin Head-Gordon,[‡] and Alexis T. Bell*[,†]

[†]Department of Chemical and Biomolecular Engineering, University of California, Berkeley, California 94720-1462

[‡]Department of Chemistry, University of California, Berkeley, California 94720-1462

Supporting Information

ABSTRACT: Ga-exchanged H-MFI zeolites are highly active for the dehydrogenation of light alkanes; however, both the nature of the active gallium species and the associated dehydrogenation mechanism have been difficult to establish. In this study, we examine the activity of Ga species in Ga/H-MFI by calculating the free energy landscapes on which all reactions occur. To this end, we use a hybrid quantum mechanics/molecular mechanics model for all electronic structure calculations. Quantum chemical calculations were carried out with a range-corrected functional and a good representation of dispersive interactions. The molecular mechanics part of our approach captures the long-range effects of Coulombic and dispersive interactions due to atoms in the extended framework. The rate-determining TS (RDTS) is identified by analysis of the free energy landscape for each mechanism, using the energetic span model. Our analysis reveals that, for reduced Ga/H-MFI, univalent and divalent gallium hydrides, $[GaH_2]^+$ and $[GaH]^{2+}$, respectively, are more active for ethane dehydrogenation in comparison to H^+ sites and Ga^+ sites. $[GaH]^{2+}$ sites consistently emerge as the most active sites for light alkane dehydrogenation, providing significant enthalpic stabilization to C−H cleavage TSs via alkyl and carbenium dehydrogenation routes. In contrast, carbenium-like C−H cleavage TSs occurring on Brønsted acid sites are enthalpically less favorable due to their limited electronic interactions with framework O atoms and H^+ sites. Activation enthalpy barriers for dehydrogenation determined using the energetic span analysis are in good agreement with those measured experimentally. Accounting for entropy of activation reveals that constrained TSs become less favorable in free energy with increasing chain length. We also find that an increase in enthalpic favorability of the alkyl mechanism is observed with increasing chain length for the TS responsible for the second C−H cleavage step leading to alkene formation.

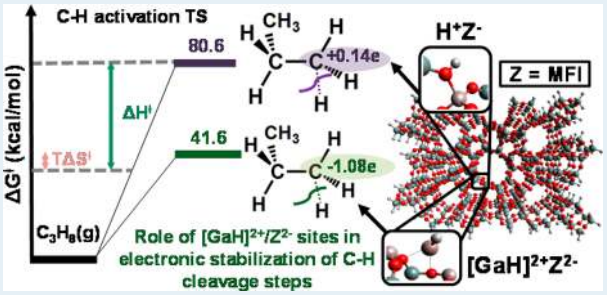

KEYWORDS: *dehydrogenation, hydrides, molecular catalysis, zeolites, DFT, light alkanes, gallium*

1. INTRODUCTION

The dehydroaromatization of C_2−C_4 light alkanes derived from naphtha cracking and natural gas is an attractive process for the production of aromatics, principally benzene, toluene, and xylene (BTX), important feedstocks for the petrochemical and fuel industries,[1,2] and there are now several commercial processes for light alkane dehydroaromatization: e.g., the Cyclar Process (developed by BP and UOP) and the Aroforming Process[2] (developed by IFP and Salutec), all of which use zeolites as catalysts. Of the various zeolites considered, MFI has been found to be particularly well suited for alkane dehydroaromatization because it has a 3-D topology and microporous structure of an intermediate size, which minimizes deactivation due to coke formation.[3] Although the protonated form of MFI, H-MFI, is capable of dehydroaromatization of light alkanes, it exhibits low selectivity due to the prevalence of undesired cracking routes.[4,5] Significant enhancement in the yield of BTX products can be achieved by modifying H-MFI with metals, such as Pt, Ru, Zn, Mo, and Ga.[6,7] Because Ga-exchanged H-MFI (Ga/H-MFI) is highly selective and stable under industrially relevant conditions for light alkane dehydroaromatization,[8] considerable effort has been devoted to understanding the structure and function of gallium species in Ga/H-MFI. The general consensus[9,10] is that both Brønsted acid and Ga-based Lewis acid sites in Ga/H-MFI are required to promote the dehydroaromatization of light alkanes.[5]

Prior studies have shown that alkane dehydroaromatization begins with alkane dehydrogenation to form alkenes, which then undergo oligomerization and dehydrogenation of the resulting products to produce aromatic compounds. Given the importance of alkane dehydrogenation as the first step in the overall dehydroaromatization process and the identification of Ga cations as the active center for promoting this initial reaction, considerable effort has been devoted to identifying the composition and structure of extraframework Ga cations and their role in the dehydrogenation of alkanes to alkenes.

Received: December 14, 2017
Revised: May 9, 2018
Published: May 15, 2018

DOI: 10.1021/acscatal.7b04295
ACS Catal. 2018, 8, 6146−6162

The structure and oxidation state of extraframework Ga species has been investigated experimentally using a variety of techniques.[11−13] EXAFS[11] characterization suggests that Ga^{3+} cations may be present as hydride species in the presence of hydrogen or ethane, such as monovalent $[GaH_2]^+$ and divalent $[GaH]^{2+}$ cations.[11] The observation of IR bands at 2040 and 2060 cm^{-1} for Ga−H stretches in $[GaH_2]^+$ and $[GaH]^{2+}$, respectively, supports the presence of these species in Ga/H-MFI under reducing conditions.[12,13] Further evidence for the formation of $[GaH_2]^+$ has been deduced from pulsed-reaction studies of propane dehydrogenation, in which it was observed that the ratio of H_2 formed to propane consumed increased and reached a value of 1:1 with an increasing number of pulses.[14] These data were interpreted to suggest that $[GaO]^+$ cations were reduced in situ by propane to form $[GaH_2]^+$, a conclusion that was supported by temperature-programmed reduction experiments.[15] The role of Ga^+ in the dehydrogenation of light alkanes has also been proposed on the basis of the observation of a low-energy feature in the Ga-edge XANES spectra of reduced Ga/H-MFI and has been extensively invoked in subsequent studies.[11,16,17] It is notable, though, that recent work has found that the observed shift in edge energy is likely due to a change in the coordination of Ga^{3+} under reducing conditions and not to the reduction of Ga^{3+} to Ga^+.[18] As a consequence, the role of Ga^+ in promoting the dehydrogenation of light alkanes is brought into question and requires further consideration.

Density functional theory (DFT) calculations have also been widely used to explore the composition of active extraframework Ga species and their relevance to light alkane dehydrogenation over Ga/H-MFI. It is notable that both reduced and oxidized Ga cations have been considered as active centers for alkane dehydrogenation by various studies. Some of the extraframework exchanged cations reported in the literature include reduced, isolated species (Ga^+, $[GaH]^{2+}$, and $[GaH_2]^+$)[19−21] and oxidized mononuclear ($[GaO]^+$[22−24] and $[GaHOH]^+$[25]) and binuclear ($[Ga_2O_2]^{2+}$ and $[Ga_2O_2H_2]^{2+}$[22−24]) species.

Early DFT studies by Pidko, Van Santen, and co-workers on reduced Ga species focused on the dehydrogenation of ethane on $[GaH_2]^+$ and Ga^+ sites using a T8 cluster modeled at the DFT/B3LYP/6-31G** level.[19] The results of this work suggest that $[GaH_2]^+$ is inactive for ethane dehydrogenation and that this species is eventually converted to Ga^+, which is predicted to be thermodynamically favored under dehydroaromatization conditions at 823 K (ΔG_{rxn} = −18 kcal/mol). Both $[GaH_2]^+$ and Ga^+ were shown to be capable of promoting ethane dehydrogenation via mechanisms involving alkyl intermediates (alkyl gallium hydrides). The predicted value of the apparent activation energy for ethane dehydrogenation was found to be significantly higher for $[GaH_2]^+$ (62 kcal/mol) than for Ga^+ (56 kcal/mol). The energetics of ethane dehydrogenation over $[GaH_2]^+$ have also been investigated using small cluster models of $[GaH_2]^+$ containing 5−22 framework tetrahedral atoms and different levels of theory by Nascimento and co-workers.[26,27] The apparent activation energies reported in these studies range from 54 to 65 kcal/mol. It is notable that all of the predicted activation barriers for ethane dehydrogenation over univalent sites ($[GaH_2]^+$ and Ga^+) are significantly larger than the experimentally measured activation barrier of 39 kcal/mol for this process on H-MFI-supported gallium oxide.[28] The authors of this experimental study also note that, for conditions where deactivation and transport effects can be ruled out, the apparent activation energy decreases to 30.5 kcal/mol, which can be attributed to the formation of well-dispersed and active Ga-exchanged sites in Ga/H-MFI upon in situ reduction.[5]

Joshi et al.[21,25] have proposed that univalent $[GaH_2]^+$ sites are inactive for ethane dehydrogenation and that dehydrogenation requires divalent $[GaH]^{2+}$ sites that charge compensate pairs of framework Al atoms in Ga/H-MFI. These Ga sites were found to be active for ethane dehydrogenation via two different types of mechanisms: carbenium and alkyl. Figure 1

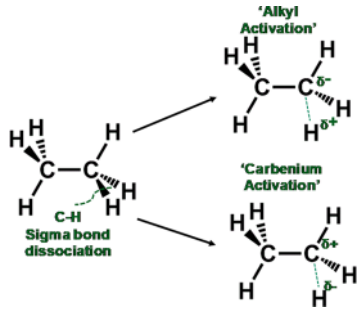

Figure 1. Illustrations of σ-C−H dissociation which can occur through either an "alkyl activation" route or a "carbenium activation" route.

shows that alkane C−H bond dissociation can lead to either a carbenium or an alkyl intermediate. C−H bond activation to form an alkyl intermediate can be envisioned as both electrons being retained on the activated carbon (α-C), whereas C−H bond activation to form a carbenium intermediate results in both electrons being retained on the hydrogen being cleaved, rather than on the α-C. Joshi et al. have proposed[21,25] that a carbenium-type mechanism involving an ethoxide intermediate is the preferred pathway for ethane dehydrogenation. Although routes involving alkyl activation were also investigated, these routes were found to have a larger activation barrier in comparison to those for the carbenium mechanism.[21,25] The authors also noted that not all framework configurations involving two Al atoms produced equally active $[GaH]^{2+}$ sites at 823 K and that, to achieve an optimal activity, the Al−Al pair combination needed to be separated by more than 0.55 nm.

The role of the distance between pairs of Al atoms has also been discussed in other theoretical studies. Pidko et al. have reported that $[GaH]^{2+}$ sites associated with distant Al atoms that are 0.81 nm apart are unstable and are likely to rearrange into Ga^+ and H^+.[19] Later DFT studies by Zhidomirov and co-workers examined oxidized Ga species[23,24,29] proposed to be present in Ga/H-MFI treated with H_2O, O_2, or N_2O.[16,30,31] The authors observed that partially reduced binuclear clusters in the form of $[Ga_2O_2H_2]^{2+}$ associated with pairs of Al atoms that are 0.72−0.75 nm apart could also be highly active for ethane dehydrogenation via alkyl Ga hydride mediated pathways.[23] The activation barriers for ethane dehydrogenation predicted in this work were found to be lower than those for reduced Ga^+ and $[GaH_2]^+$ sites but closer to the values predicted by Joshi and Thomson for active $[GaH]^{2+}$ sites in the aforementioned studies.

The preceding discussion shows that both oxidized and reduced forms of Ga have been found to be active for alkane dehydrogenation, and the mechanism by which this reaction occurs has been analyzed via DFT calculations. It should be noted, though, that only reduced sites have been found under the conditions where Ga/H-MFI is utilized for light alkane dehydroaromatization,[5,12,32] whereas oxidized sites[23,33−37] (e.g.,

DOI: 10.1021/acscatal.7b04295
ACS Catal. 2018, 8, 6146−6162

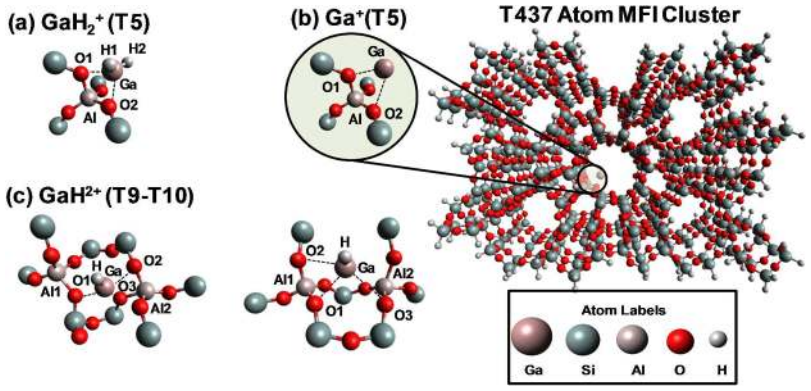

Figure 2. View along the [010] axis of T437 atom MFI structure used to model gallium-exchanged sites in Ga/HMFI: (a) $[GaH_2]^+$; (b) Ga^+; (c) $[GaH]^{2+}$. Two different Al-pair configurations (A and B) have been chosen on the basis of different Al−Al distances. Configuration A is modeled using a T10 cluster, while configuration B is modeled using a T9 cluster.

$[Ga_2O_2]^{2+}$, $[GaO]^+$, $[Ga_2O_2H_2]^{2+}$) are only stable in the presence of H_2O, O_2, or N_2O,[16,30,31] and such sites undergo reduction under reaction conditions used for dehydroaromatization.[5,38] However, even for reduced Ga sites there is a lack of consensus regarding which species (e.g., Ga^+, $[GaH_2]^+$, and $[GaH]^{2+}$) are most active and the mechanism (i.e., alkyl versus carbenium) by which the dehydrogenation of ethane and other light alkanes occurs on Ga/H-MFI. A closely related question not addressed in previous theoretical studies is the extent to which the conclusions drawn are a consequence of the choice of cluster used to represent the zeolite as well as the level of theory used. These are relevant issues, since previous studies have shown that calculated activation barriers can decrease by as much as 15 kcal/mol when the number of atoms in the cluster used to represent the zeolite is increased for a given level of theory.[39] The noted decrease in the activation energy is a consequence of stabilization of the transition state relative to the reactant state due to long-range electrostatic and van der Waals interactions of atoms near the active center with atoms in the extended zeolite framework.[20,40,41] A review addressing these effects on adsorption and reactions occurring in zeolites can be found in ref 42. Another critical issue with previous DFT studies of alkane dehydrogenation over Ga/H-MFI is that the predicted activation barriers have been determined solely from an analysis of the potential energy landscape, but not the free energy landscape. This is a serious omission, since the role of entropy in determining the rate-limiting step can be significant,[43] especially for reactions occurring at the temperatures of interest for light alkane dehydroaromatization (823 K).

In the present study, we employ a long-range corrected, hybrid quantum mechanics/molecular mechanics (QM/MM) approach to examine the nature of various reduced Ga species in MFI and their activities for the dehydrogenation of light alkanes. We have previously shown that QM/MM calculations are both accurate and cost-effective tools for predicting enthalpy changes for molecular adsorption and activation barriers for elementary reaction steps occurring in MFI and other zeolites.[42,44,45] The primary objectives of this study are to elucidate the nature and activity of reduced Ga species in Ga/H-MFI for light alkane dehydrogenation, including identification of the preferred free energy pathway for this reaction over different Ga species and the dependence of the preferred pathway on alkane chain length. We have limited this work to reduced Ga species, since these are the species for alkane dehydrogenation occurring as the first step of alkane dehydroaromatization, a subject that we will address in future communications.

2. THEORETICAL APPROACH

2.1. Zeolite Model Description. The hybrid QM/MM approach used in this work has been described in detail previously.[46,47] This approach takes into account the effect of long-range dispersive interactions and the polarization of the active site by the electrostatic field associated with the zeolite lattice, both of which are critical to capturing reaction energetics accurately. A T437 atom cluster is used to represent the zeolite framework surrounding the active site. The QM region consists of either a T5 or a T9-T10 cluster representing the part of the zeolite associated with the Ga cation (Ga^+ or $[Ga(H)_n]^{(3-n)+}$) and any adsorbed species. The MM region contains Si and O atoms that are fixed at their crystallographic positions; the associated Lennard−Jones parameters and fixed nonpolarizable charges used to describe the effects of dispersive and Coulombic interactions were taken from ref 48.

Four Lewis acidic sites were examined for their stability and dehydrogenation activity, all of which are shown in Figure 2. Two of these sites are univalent, $[GaH_2]^+$ and Ga^+, the former being tetrahedrally coordinated to two framework oxygens and two hydride ions and the latter coordinated to only two framework oxygen atoms. The framework Al atom associated with these extraframework sites is taken to be at the T12 site, which has been found to be a favorable location for Al atoms in the channel intersections of MFI.[49] As noted in section 4, we use the same model to investigate light alkane dehydrogenation over a Brønsted acid site model. The next Lewis acid site considered is the divalent $[GaH]^{2+}$ cation, which charge-compensates a pair of Al atoms in the MFI framework. For this site, the T5 QM region is extended to a T9-T10 region, as illustrated in Figure 2. As shown previously, only a small difference (2.6 kcal/mol) was found in the calculated barriers for ethene methylation over H-MFI calculated for both T5 and T20 clusters,[50] which suggests that our QM/MM approach is not significantly influenced by the size of the QM region used. The positioning of the first configuration (A) of the $[GaH]^{2+}$ cation within this cluster is based on the work of Joshi et al.,[21] who studied the effect of Al−Al distances on the activity of $[GaH]^{2+}$ for ethane dehydrogenation. On the basis of this study, one optimal Al−Al pair is located in an 8-MR located close to the channel intersection at an Al−Al distance of 0.57

DOI: 10.1021/acscatal.7b04295
ACS Catal. 2018, 8, 6146−6162

nm, as illustrated in Figure 3. A second configuration of $[GaH]^{2+}$ (B) was examined as well (see Table S24 for four

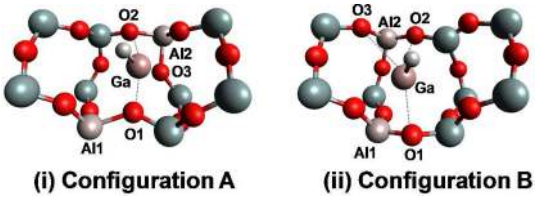

Figure 3. Al−Al pair configurations used to model $[GaH]^{2+}$ for site stability and activity analyses in this work. Configuration A is separated by an Al−Al distance of 0.57 nm, while configuration B is separated by 0.49 nm. Only the 8-MR/6-MR from the QM/MM model has been displayed here for illustration purposes.

different Al−Al configurations sampled). Configuration B, which is expected to be more stable than configuration A, is also located within the 8-MR, but the Al−Al distance is now 0.49 nm although the same types of T sites, as in configuration A (T07 and T12), are involved. This configuration (B) of $[GaH]^{2+}$ is more closely coordinated to zeolitic oxygens, which leads to a more stable $[GaH]^{2+}$ structure.

2.2. Computational Details. Stationary and saddle point searches were conducted at the ωB97X-D/6-31G** level of theory using the default optimization procedure available in QChem.[51] Guesses for saddle-point searches were obtained using the freezing string method[52] or were generated manually. Intrinsic reaction coordinate (IRC) searches were used to confirm the validity of the first-order saddle points on a minimum energy path connecting the reactant and product intermediates within the mechanism of interest. The reported activation energies were computed using the ωB97X-D functional[53] with the triple-ζ, split-valence Pople basis set, with diffuse and polarization functions 6-311++G(3df,3pd). ωB97X-D is a range-separated hybrid functional, which has performed well in recent large-scale assessments of the accuracy of density functionals,[54,55] and has also performed very well for evaluation of relative energies in previous QM/MM studies of zeolites.[42,44,46,48,50,56,57] Furthermore, the most attractive feature of this approach is its cost effectiveness and versatility. Gomes et al.[50] have estimated that an improvement of nearly 3 orders of magnitude can be achieved by using a QM(T5)/MM(437) cluster in lieu of a full QM T44 region at the ωB97X-D/6-311++G(3df,3pd) level of theory. Partial charges, wherever reported, were computed using natural bond orbital (NBO) analysis,[58] and all calculations were performed using a developmental version of QChem Software.[59]

2.3. Free Energy Calculations and Catalytic Cycle Analysis. Free energy calculations, which are used to perform a first-principles-based catalytic cycle analysis in this work, are reported at 823 K and 1 atm, typical conditions used in experimental studies of light alkane dehydroaromatization. Enthalpy and entropy calculations were performed using the partition functions derived for the rigid rotor harmonic oscillator (RRHO) approximation. Soft modes with small vibrational frequencies are known to yield inaccurate entropy and free energy predictions using this RRHO approximation.[60,61] To remedy this issue, we used a quasi-RRHO model, in which an interpolation is made between a free rotor at lower frequencies and a harmonic oscillator at higher frequencies using a frequency-dependent weighting function.[62] We have used this approach successfully in previous work to obtain activation enthalpies and entropies for *n*-butane reactions in H-MFI, yielding good agreement with experimental results.[63]

As many of the dehydrogenation mechanisms investigated in our study involve multiple steps, the step which governs the rate of reaction on a given site is determined by analysis of the free energy surface using the first-principles-based energetic span model proposed by Kozuch and Shaik.[64−67] In this approach, the turnover frequency for a catalyzed reaction is governed by the transition state and intermediate which maximize the energetic span of a given catalytic cycle. This energetic span is determined by examining the free energy surface for the highest summit and the lowest trough, and it provides an estimate of the apparent free energy of activation ($\Delta G^{\ddagger}$) which has to be overcome in order to complete a given catalytic cycle. For each mechanism reported, we determine the value of $\Delta G^{\ddagger}$ from the respective free energy surface using this approach to determine which site provides the most facile dehydrogenation route.

We note as well that, on each free energy profile, the highest summit and the lowest troughs are colored green, with energies labeled in a box to illustrate the rate-determining energetic span for a given catalytic cycle. In addition, the free energy surfaces reported in our results were labeled only for the key surface intermediates relevant to the chemistry of a given step. Therefore, for each of the structures, all of the gas-phase species that desorb during the course of the reaction (e.g., alkene and dihydrogen) are accounted for in the calculations but are not marked on the free energy profile for the sake of clarity. The zero-point corrected enthalpy and free energy values for all of the mechanisms investigated in our work can be found in Tables S1−S23 in the Supporting Information.

3. NATURE OF SITES AND DEHYDROGENATION MECHANISMS

3.1. Site Stability and Interconversion. An important consideration in our analysis is the stability of each gallium species and the possibility that site interconversion can occur. To this end, the activation barriers for the transition states which convert $[GaH_2]^+$ to Ga^+ via reductive elimination and also $[GaH]^{2+}$ to $[GaH_2]^+$ via H_2 disproportionation are illustrated in Figures 4 and 5. We note that ,while it has been suggested that $[GaH_2]^+$ is trapped kinetically,[13,68] the magnitude of the free energy barrier for the conversion of this species to Ga^+ has not been reported in earlier theoretical studies, which only cite the thermodynamic favorability of Ga^+ formation.[19] In Figure 4, we report the free energy barrier for

Figure 4. Example of one possible transition state structure predicted for reductive elimination which transforms $[GaH_2]^+$ to Ga^+. Respective kinetic and thermodynamic free energy barriers for site interconversion are reported at 823 K and 1 atm. Although this homopolar H_2 formation suggests that there may be a kinetic barrier to Ga^+ formation, more electronically facile TSs may lead to Ga^+ formation. Only the QM region from the QM/MM model has been displayed here for illustration purposes.

DOI: 10.1021/acscatal.7b04295
ACS Catal. 2018, 8, 6146−6162

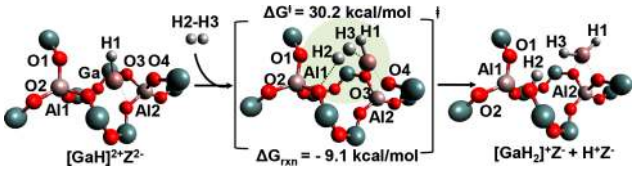

Figure 5. Transition state structures predicted for conversion of $[GaH]^{2+}$ (configuration A) to $[GaH_2]^+$ and H^+ sites via H_2 disproportionation. Respective kinetic and thermodynamic free energy barriers for site interconversion are reported at 823 K and 1 atm. Only the QM region from the QM/MM model has been displayed here for illustration purposes.

converting $[GaH_2]^+$ to Ga^+; the high value for this kinetic barrier (79 kcal/mol) appears to be consistent with the aforementioned proposal[68] that $[GaH_2]^+$ may be kinetically trapped[13] at high temperatures despite the thermodynamically favored formation of Ga^+. However, we note that there may, in theory, be other pathways that are electronically more favorable than the homopolar process shown here: for instance, a heteropolar reductive elimination or direct rearrangement of $[GaH]^{2+}$ into Ga^+ and H^+ without involvement of $[GaH_2]^+$.[19] As such transition states have not been observed as saddle points on the potential and free energy surfaces for site interconversion between various Ga species, whether they exist or not remains an open question. Therefore, it is unclear both from theoretical and experimental results whether $[GaH_2]^+$ is trapped kinetically and, hence, does not form Ga^+ under the reaction conditions. To provide a complete analysis of dehydrogenation on univalent sites, we examine the dehydrogenation of ethane on both $[GaH_2]^+$ and Ga^+ sites in section 3.2.

Figure 5 illustrates that the free energy of reaction for the conversion of the $[GaH]^{2+}$ in configuration A to $[GaH_2]^+$ and H^+ in the presence of H_2 is favorable thermodynamically and quite feasible kinetically (ΔG_{rxn} = −9.1 kcal/mol; $\Delta G^{\ddagger}$ = 30.2 kcal/mol). The negative free energy of this reaction alone is enough to render the presence of $[GaH]^{2+}$ cations in configuration A unlikely thermodynamically.[69] It is also notable that the free energy barrier for the reaction $[GaH]^{2+} + H_2 \rightarrow [GaH_2]^+ + H^+$ (30.2 kcal/mol) renders this site conversion pathway relatively facile. Furthermore, since the gas phase under the conditions of alkane dehydroaromatization is expected to contain substantial quantities of H_2, the high fugacities of H_2 within the zeolite would lead to a significant thermodynamic conversion for this reaction, suggesting that $[GaH]^{2+}$ cations in configuration A are less likely to exist under the reaction conditions (under an alkane- or H_2-rich, reducing environment), despite being highly active (see Text S1 for details). For example, even in the presence of only 0.1 atm of H_2, the expected thermodynamic conversion of such $[GaH]^{2+}$ sites to $[GaH_2]^+$ and H^+ is estimated to be at least 96%, and this number renders the presence of the former cation in configuration A less likely, as the partial pressures of H_2 under the reaction conditions are typically on the order of 0.1 atm of H_2.[2,70]

On the other hand, $[GaH]^{2+}$ cations in configuration B (ΔG_{rxn} = 6.6 kcal/mol for H_2 disproportionation into $[GaH_2]^+$ and H^+, as shown in Table S24) are expected to be more stable due to thermodynamically limited conversion into $[GaH_2]^+$ and H^+ under the reaction conditions, in comparison with $[GaH]^{2+}$

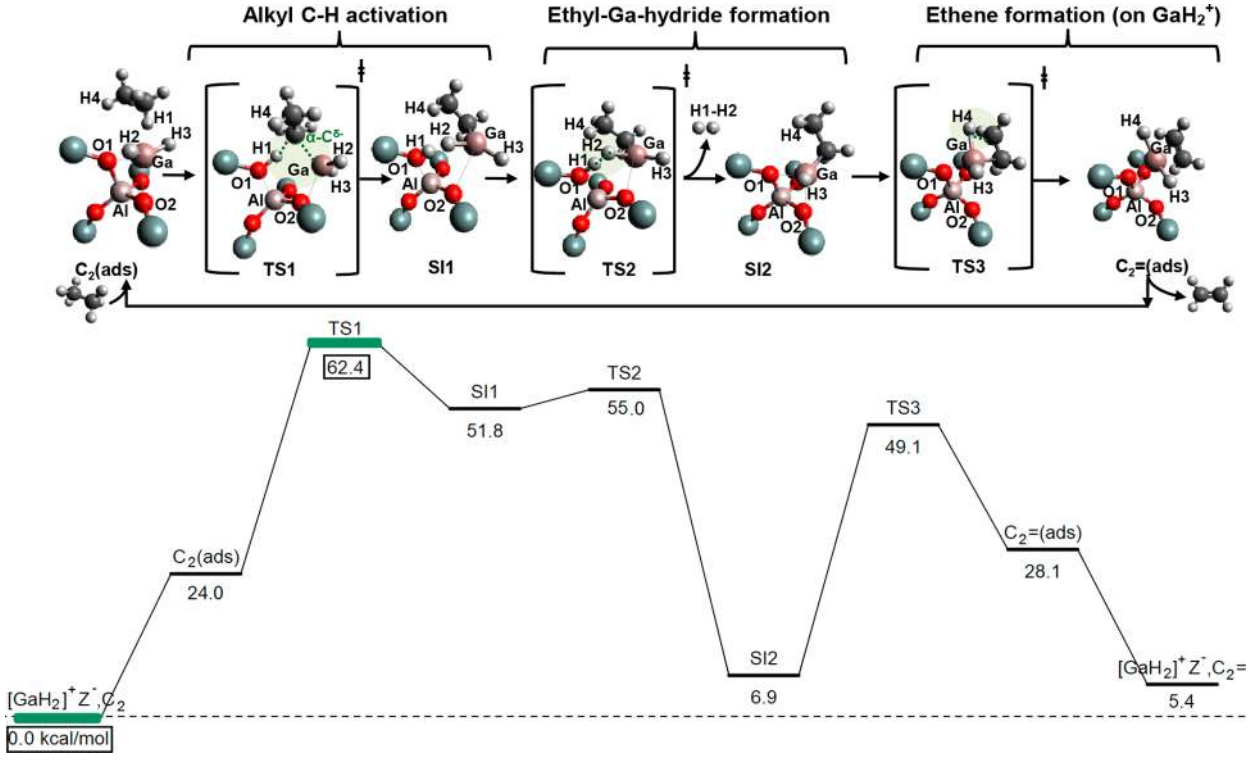

Figure 6. Ethane dehydrogenation via a stepwise alkyl mechanism on $[GaH_2]^+$ and the corresponding free energy surface (kcal/mol) reported at 823 K and 1 atm. The free energy span-determining states are labeled in green, with energies marked in rectangles, as shown by the highest-lying rate-determining transition state (RDTS) and lowest lying resting state. Only the QM region from the QM/MM model has been displayed here to illustrate the elementary steps in this mechanism.

DOI: 10.1021/acscatal.7b04295
ACS Catal. 2018, 8, 6146−6162

cations in configuration A. Therefore, as cations in configuration B are likely to be more representative of the $[GaH]^{2+}$ sites present during actual ethane dehydrogenation conditions in Ga/H-MFI, all discussions of $[GaH]^{2+}$ sites in the subsequent sections of this work pertain to more stable $[GaH]^{2+}$ sites in configuration B. The energetic span analyses conducted on less stable but highly active $[GaH]^{2+}$ sites of configuration A, along with their associated dehydrogenation mechanisms, can be found in Text S1.

3.2. Ethane Dehydrogenation on $[GaH_2]^+$ Sites. *3.2.1. Stepwise Alkyl Mechanism.* The stepwise alkyl mechanism was first proposed by Frash and Van Santen, who refer to it as the "three step mechanism".[71] We refer to this mechanism as the stepwise alkyl mechanism, to distinguish it from other "carbenium" and "concerted" (single-step) mechanisms. The "alkyl" character of the α-C is maintained throughout the reaction cycle in this mechanism.[71] Figure 6 shows that the stepwise alkyl mechanism on $[GaH_2]^+$ proceeds via three steps following ethane adsorption. In the first step, heterolytic alkyl activation of a C−H bond leads to the formation of an alkyl intermediate (SI1) and a Brønsted acid site on the zeolite surface ($H1^+$ on O1) via TS1. In the second step, ethyl Ga hydride formation occurs via transfer of a hydride ($H2^-$) to $H1^+$, which leads to the release of H_2 via TS2. Finally, in the third step, ethene is formed by transfer of $H4^-$ (cleaved from the ethyl fragment) to the gallium center, thereby completing the catalytic cycle. Our calculations predict that the catalytic cycle for the stepwise alkyl mechanism on $[GaH_2]^+$ occurs with an apparent free energy barrier (based on the energetic span analysis) of 62.4 kcal/mol, associated with TS1. The high free energy barrier for TS1 can be attributed to the large entropic penalty associated with this TS in comparison to other TSs in this mechanism. The motion of the alkyl fragment is severely limited, as it is bound at two locations on the zeolite surface: to both the gallium center and the proton.

Table 1 gives the vibrational frequencies calculated for the ethyl Ga hydride intermediate. This species has been observed by DRIFTS[12] when ethane is passed over Ga/H-MFI at 673 K. As can be seen from Table 1, the unscaled frequencies are in reasonable agreement with those observed experimentally, especially for all the Ga−H vibrations. This experimental observation of the $[H-Ga-C_2H_5]^+$ intermediates during ethane flow over Ga/H-MFI provides experimental support for the relevance of the stepwise alkyl mechanism for ethane dehydrogenation on Ga/H-MFI. The stretching frequencies reported in parentheses for the ethyl fragment in $[H-Ga-C_2H_5]^+$ have been scaled by factors[72] determined using benchmarked data (ωB97X-D/6-311G**) for a test set of known molecules such as ethane and are therefore in better agreement with the experimentally observed IR bands.

Table 1. Comparison of Harmonic Wavenumbers Calculated via QM/MM and Measured Using DRIFTS

species	mode	$\nu_{QM/MM}$ (cm^{-1})[a]	ν_{exp} (cm^{-1})	ref
$[GaH_2]^+$	Ga−H (asym stretch)	2043	2041	12, 13
	Ga−H (bend)	929	953	73
$[H-Ga-C_2H_5]^+$	Ga−H (stretch)	2048	2057	73
	C−H (stretch) in $-C_2H_5$	3041 (2910)	2882	13
		3050 (2919)	2914	13
		3115 (2981)	2939	13
		3155 (3019)	2963	13
$[GaH]^{2+}$	Ga−H (stretch)	2059	2057	12, 13

[a]Scaled frequencies reported in parentheses.

Ga−H stretches in both $[GaH]^{2+}$ and $[GaH_2]^+$ species are observed when hydrogen is passed over Ga/H-MFI[13] at 773 K, and therefore calculations for these modes have also been shown in Table 1 for comparison. The Ga−H stretching frequency observed for $[GaH_2]^+$ is also in good agreement with the experimentally reported band for this cation.[12,13,73] Since IR studies show that $[GaH_2]^+$ is also observed both in a hydrogen-rich, reducing environment and in the presence of flowing ethane,[74,13] the $[GaH_2]^+$ cation is predicted to be stable under hydrogen-rich, ethane reaction conditions.

3.2.2. Concerted Mechanism. The concerted dehydrogenation mechanism was first proposed by Pereira et al.[27] and is shown in Figure 7. This pathway involves simultaneous C−H activation and ethene desorption within a single transition state. Figure 7 illustrates the formation of dihydrogen (via the combination of $H2^-$ and $H3^+$) and the simultaneous release of ethene by the transfer of $H4^-$ to the Ga center. The principal difference between the concerted transition state appearing in Figure 7 and the transition states for the stepwise alkyl mechanism appearing in Figure 6 is the lack of direct involvement of the Ga center in the change in hybridization undergone by the α-C from sp^3 in ethane to sp^2 in ethene. In contrast to the Ga center in the stepwise alkyl mechanism, the Ga center in the concerted mechanism does not directly stabilize the α-C during C−H activation. The lack of such direct participation by Ga^{3+} in the concerted mechanism is one of the reasons the free energy barrier, 86.1 kcal/mol (based on the energy span analysis), for dehydrogenation via the concerted mechanism is higher by 23.7 kcal/mol than that for the stepwise alkyl mechanism.

Another factor contributing to the high barrier for the concerted mechanism is the lack of zeolite framework assisted steps, which facilitate hydrogen transfer, as seen in the more facile stepwise-alkyl mechanism. The lack of framework-assisted transfers precludes transition-state stabilization by the extended lattice, leading to higher electronic barriers. Both of these factors contribute to the higher free energy of activation associated with the concerted pathway, suggesting that it does not compete with the more facile, stepwise alkyl mechanism for ethane dehydrogenation on $[GaH_2]^+$.

3.3. Ethane Dehydrogenation on $[GaH]^{2+}$ Sites. Much of the chemistry described in this section builds on the work of Joshi et al.,[21] who examined two distinct mechanisms for ethane dehydrogenation on $[GaH]^{2+}$—the carbenium and the alkyl mechanism. In the former case, the α-C is polarized positively ($C^{\delta+}$) to form carbenium-like intermediates and transition states, while in the latter case, the α-C is polarized negatively ($C^{\delta-}$) to form carbanion-like, alkyl intermediates and transition states (see Figure 1). Illustrations of the adsorption modes governing whether alkyl or carbenium chemistry occurs on $[GaH]^{2+}$ and key atomic distances are shown in Table 2. In the carbenium adsorption mode, H1 is closer to the Ga center than is H1 in the alkyl mode, while the α-C is closer in the latter mode to the Ga center, which enables the formation of alkyl-type transition states and intermediates. The carbenium adsorption mode facilitates the formation of a carbenium-type transition state by interaction of the α-C with a zeolitic oxygen

DOI: 10.1021/acscatal.7b04295
ACS Catal. 2018, 8, 6146−6162

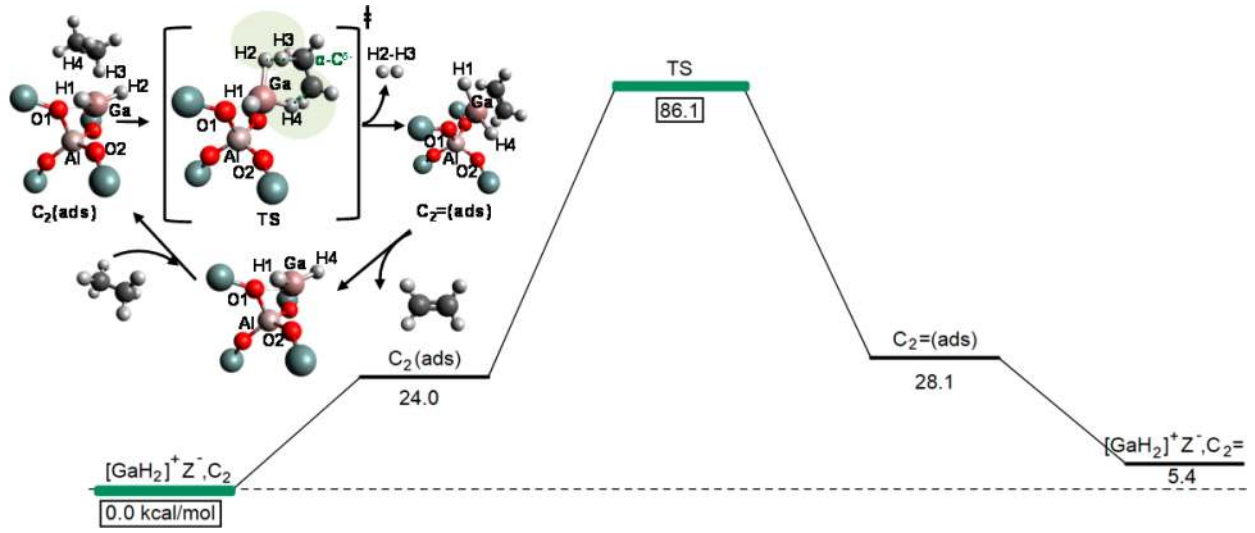

Figure 7. Ethane dehydrogenation via the concerted mechanism on $[GaH_2]^+$ and the corresponding free energy surface (kcal/mol) reported at 823 K and 1 atm. The free energy span-determining states are labeled in green, with energies marked in rectangles, as shown by the highest-lying rate-determining transition state (RDTS) and lowest-lying resting state. Only the QM region from the QM/MM model has been displayed here to illustrate the elementary steps in this mechanism.

Table 2. Depiction of Geometric Differences between Carbenium and Alkyl Adsorption Modes on $[GaH]^{2+}$ in Terms of Atomic Distances (Å)[a]

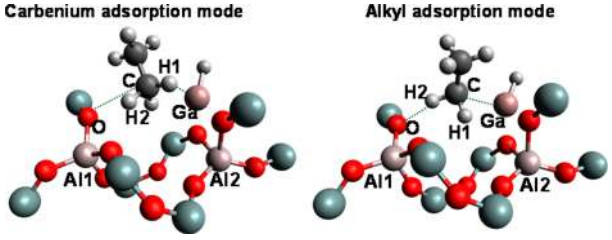

	adsorption mode on $[GaH]^{2+}$	
bond distance (Å)	carbenium	alkyl
C−H1	1.123	1.108
C−Ga	2.398	2.300
H1−Ga	2.011	2.143
O−H2	2.115	1.992

[a]The carbenium adsorption mode situates the dissociating H1 from the activated C−H1 bond closer to the Ga center, facilitating a carbenium activation of the activated α-C. On the other hand, the alkyl adsorption mode situates the α-C closer to the Ga-center, facilitating alkyl activation. Only the QM region from the QM/MM model has been displayed here for illustration purposes. Structures shown above were generated on $[GaH]^{2+}$ cations in configuration B.

atom. This TS then leads to carbenium-type intermediates, as discussed in section 3.3.1.

3.3.1. Carbenium Mechanism. Ethane dehydrogenation via the carbenium route on $[GaH]^{2+}$ involves multiple steps, as shown in Figure 8. Ethane first adsorbs onto the site via a "carbenium mode", in which the α-C is situated closer to the zeolitic oxygen than to the gallium monohydride; this adsorption mode is facilitated by the steric hindrance from the methyl group, blocking the access of the α-C to the Ga^{3+} center.[21] The reaction is initiated via TS1 (carbenium C−H activation) by the transfer of a hydride ($H2^-$) from this methyl group to the Ga^{3+} center, to yield the monovalent $[GaH_2]^+$ cation, which charge-compensates the first framework Al atom, Al1. This step, which proceeds via TS1, involves the incipient formation of an ethoxide which subsequently attaches to the zeolitic oxygen O4, thereby compensating the charge associated with the second framework Al atom, Al2.

An interesting feature of TS1 is the small amount of positive charge on the α-C: +0.002e, which is much lower than that typically expected for reactions proceeding via a carbenium mechanism. The positive charge has previously been calculated to be 2 orders of magnitude higher in previous work.[71] The observed diminishment of the carbenium character of the C−H activation transition indicates that there is an electron-sharing effect that can be attributed to the interaction of the activated α-C with the basic zeolitic oxygen, O4, associated with the second Al site (Al2); this interaction with the zeolitic oxygen decreases the carbenium character of the transition state to the extent that it is now barely carbocationic in nature.

Since C has an electronegativity higher than that of H by 0.35 Pauling unit,[75] the α-C is expected to preferentially form a less carbenium like transition state. A less carbenium like transition state maximizes the electronic charge around the α-C, thereby reducing its positive charge, consequently stabilizing the overall electronic structure of the C−H activation TS, as the tendency of the C to attract more electrons in comparison to H is satisfied. As a result, the C−H activation TS is stabilized on the electronic and free energy surfaces for this mechanism, leading to a facile σ-C−H bond activation TS during dehydrogenation. This decrease in the carbenium character of the TS suggests that charge transfer between the O atoms in the zeolite framework and the TS for C−H cleavage is important in stabilizing the TS.

After the formation of the zeolitic oxygen bound ethoxide (SI1), a noncyclic transition state (TS2) is formed, followed by other framework-assisted steps, as shown in Figure 8. Note that this "noncyclic transition state" is distinguished by its name from other cyclic transition states, which simultaneously form ethene and dihydrogen in a concerted fashion. Conversely, the noncyclic transition state releases only ethene, while dihydrogen is released in subsequent steps. By crossing this noncyclic transition state, TS2, the zeolite now accepts a proton

DOI: 10.1021/acscatal.7b04295
ACS Catal. 2018, 8, 6146−6162

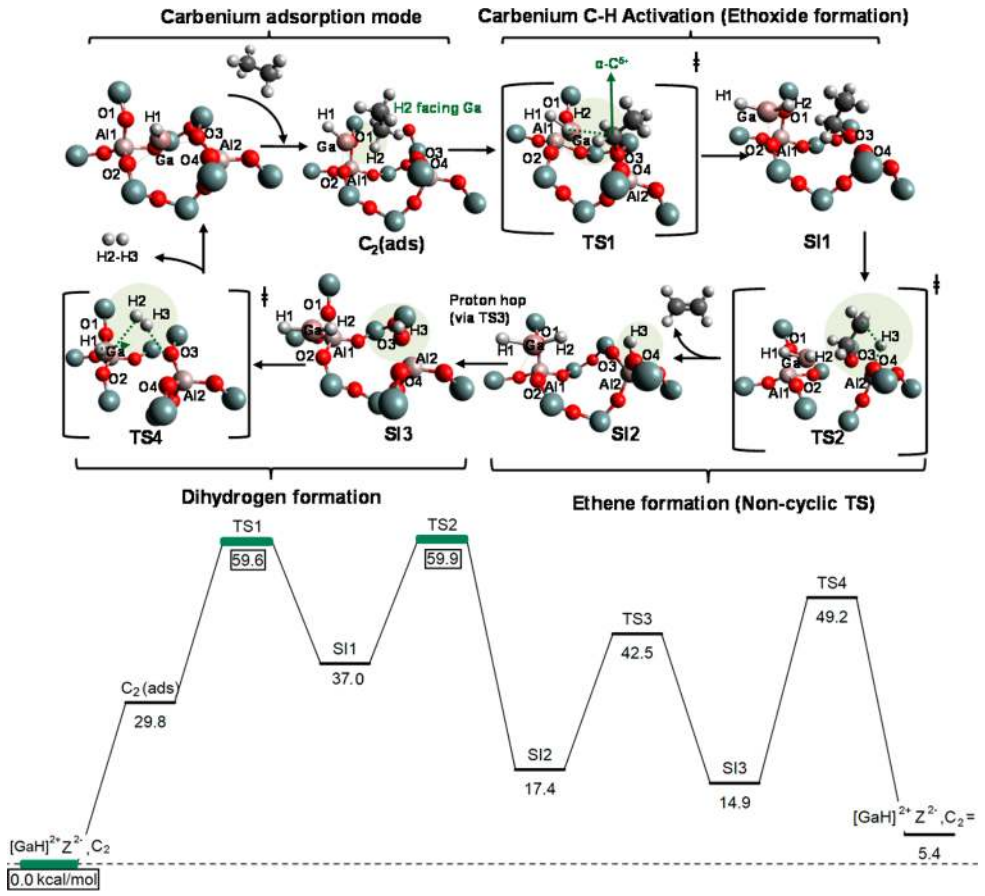

Figure 8. Ethane dehydrogenation via the carbenium mechanism (noncyclic route) on $[GaH]^{2+}$ (configuration B) and the corresponding free energy surface (kcal/mol) reported at 823 K and 1 atm. The free energy span-determining states are labeled in green, with energies marked in rectangles, as shown by the highest-lying rate-determining transition state (RDTS) and lowest-lying resting state. Only the QM region from the QM/MM model has been displayed here to illustrate the elementary steps in this mechanism. Structures illustrated above were generated on $[GaH]^{2+}$ sites of configuration B.

($H3^+$) from the second C (β-C) on the ethoxide backbone, as this β-C atom simultaneously changes hybridization, during the course of releasing ethene. The acceptance of the proton by the zeolitic oxygen, O3, converts the ethoxide to ethene. It is notable that the formation of transition state TS2 would not be possible without the mobility of atoms on the zeolite surface connected to the framework aluminum atom (Al2).

The next step in the carbenium pathway involves the formation of dihydrogen, which eventually desorbs to regenerate $[GaH]^{2+}$. As reported by Joshi et al.,[23] we find that this step is assisted by proton migration of $H3^+$ (TS3, shown on the free energy surface), which migrates from O3 to O4 (the oxygen atom closest to $[GaH_2]^+$). It should be noted that, for ethane dehydrogenation via this pathway on $[GaH]^{2+}$, there are two rate-determining TS structures, carbenium C−H activation (TS1) and ethene formation (TS2), which both have comparable energies: 59.6 kcal/mol for TS1 and 59.9 kcal/mol for TS2.

3.3.2. Alkyl Mechanism. An alkyl-type pathway for ethane dehydrogenation on $[GaH]^{2+}$ is also feasible.[19,21] Figure 9 illustrates that this reaction mechanism is initiated by the formation of an alkyl mode,[21] for which the α-C of the adsorbed ethane points toward the Ga atom in $[GaH]^{2+}$ (as also illustrated earlier in Table 2). This step is followed by alkyl C−H activation, coupled with the formation of an ethyl Ga hydride species (via TS1) along with a Brønsted acid site ($H2^+$), resulting in intermediate SI1. The activation of the C−H bond is very similar to the heterolytic alkyl C−H activation discussed in section 3.2, the only difference being that $H2^+$ forms on O4, rather than on O1 (the oxygen atom adjacent to Ga center). The next step involves a cyclic alkyl transition state for ethene formation (TS2). The formation of TS2 involves the transfer of $H3^-$ from the β-C to a Brønsted acid ($H2^+$) site while simultaneously forming ethene and dihydrogen, as the α- and β-C atoms change their hybridization from sp^3 to sp^2. Since the alkyl activation in this mechanism is electronically favored due to the higher electronegativity of the activated C (relative to H), TS1 is not energetically demanding. However, the formation of ethene from the ethyl gallium hydride intermediate (in SI1) presents a significant bottleneck of 68.4 kcal/mol at TS2 in this case and is therefore the energy span for this catalytic cycle.

3.4. Ethane Dehydrogenation on Ga^+ Sites. Figure 10 illustrates the alkyl mechanism for ethane dehydrogenation on Ga^+, which is named for the "alkyl" character of the negatively polarized α-C. As shown in Figure 10, the first step following ethane adsorption onto Ga^+ is heterolytic dissociation of a C−H bond. For this process, the α-C (labeled $C^{\delta-}$) retains both electrons at the same time that a Brønsted acid site ($H1^+$) forms on the zeolitic oxygen (O1) via TS1.

The formation of the ethyl Ga intermediate (SI1) involves the transfer of $H1^+$ formed in step 1 to the first surface

DOI: 10.1021/acscatal.7b04295
ACS Catal. 2018, 8, 6146−6162

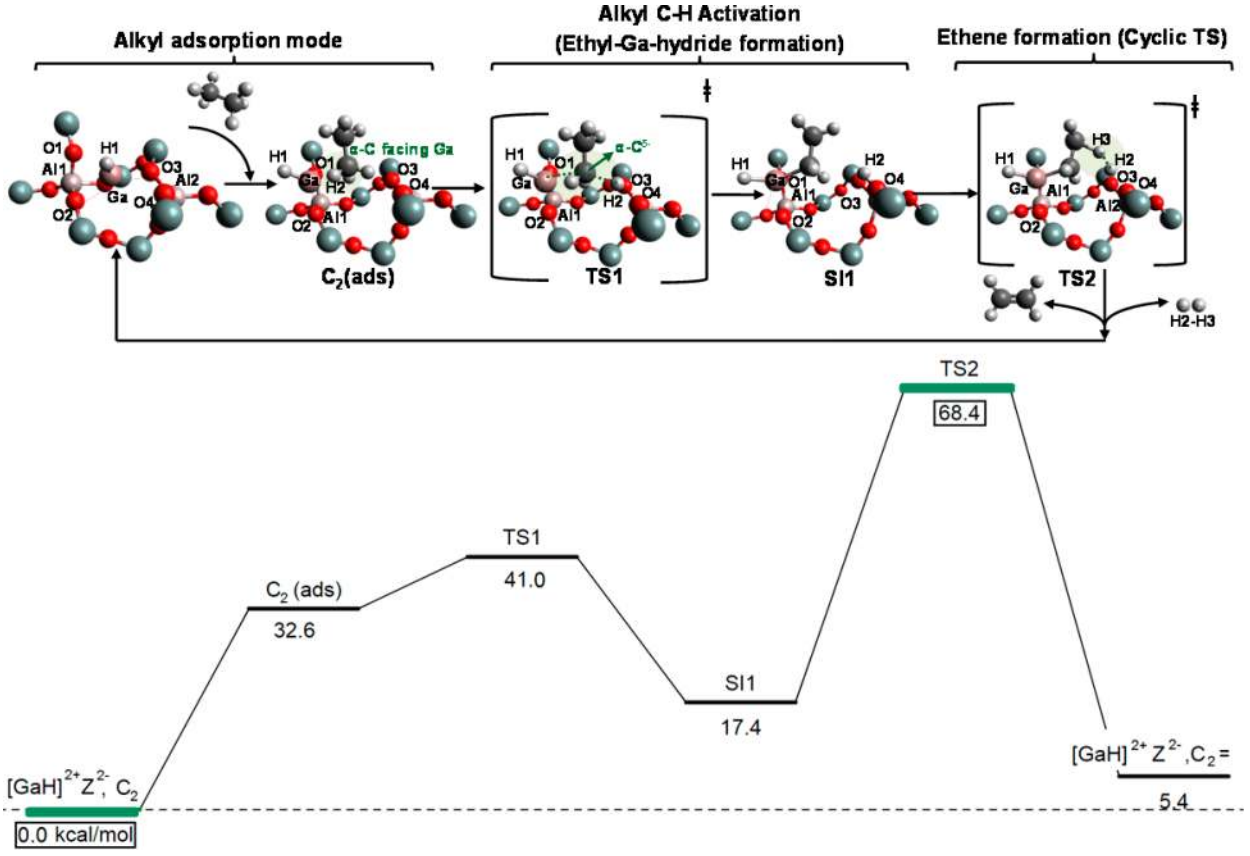

Figure 9. Ethane dehydrogenation via the alkyl mechanism (cyclic route) on $[GaH]^{2+}$ (configuration B) and the corresponding free energy surface (kcal/mol) reported at 823 K and 1 atm. The free energy span-determining states are labeled in green, with energies marked in rectangles, as shown by the highest-lying rate-determining transition state (RDTS) and lowest-lying resting state. Only the QM region from the QM/MM model has been displayed here to illustrate the elementary steps in this mechanism. Structures illustrated above were generated on $[GaH]^{2+}$ sites of configuration B.

intermediate, SI1, via TS2, a transition state, which also involves the reorientation of the ethyl fragment to a more stable configuration in the ethyl Ga hydride intermediate (SI2). The third step leads to adsorbed ethene (C_2=(ads)), which occurs via TS3. In this reaction, H1$^-$ is transferred from the gallium center to H2$^+$ (that is cleaved from the ethyl fragment) in order to release H_2. Using the energetic span analysis, we estimate that the apparent free energy of activation (marked in green) for ethane dehydrogenation via the alkyl mechanism is 80.7 kcal/mol. The activation barrier for C−H activation is higher on Ga^+ than on $[GaH_2]^+$ or $[GaH]^{2+}$ because the resting state for Ga^+ is energetically favored at 823 K, leading to higher free energy penalties for C−H cleavage TSs. Moreover, as TS1 in Figure 10 is bound to the zeolite surface in a bidentate fashion (both to the incipient H^+ and also to the Ga center), it is therefore quite constrained in its motion, which entails additional entropic losses in comparison with Ga^+, a resting state that has no adsorbed species to begin with.

Furthermore, this RDTS (TS1 in Figure 10) has a higher enthalpic barrier for C−H activation in comparison to the RDTS on $[GaH_2]^+$ (see Tables S1 and S2), which is likely linked to the Ga center in this structure not existing in its electronically favorable tetrahedral coordination. Conversely on $[GaH_2]^+$, the RDTS (TS1 in Figure 6), although similarly constrained, is closer to its preferred sp^3 coordination and therefore is better stabilized by its interaction with the Lewis basic zeolite framework O atoms than is TS1 in Figure 10. As a result, higher free energy barriers for the RDTS on univalent Ga sites are observed due to higher entropic losses and enthalpic penalties, in comparison with RDTSs on gallium hydride sites. It should be noted that the barrier associated with TS1 is only 1.4 kcal/mol lower than that associated with TS3 (79.3 kcal/mol) at 823 K, suggesting that TS3 (also marked in green) competes with TS1 as the RDTS for this catalytic cycle. Since the free energy spans associated with this mechanism on Ga^+ are considerably higher than any of the free energy spans reported in sections 3.2 and 3.3, this site is inactive for ethane dehydrogenation in comparison with Ga hydride species. In earlier studies which did not include the effect of long-range lattice electrostatics and entropy, Ga^+ sites were found to be active and were reported to have a lower barrier for alkene formation from alkyl Ga hydrides. In contrast, we observe that ethyl Ga hydrides favor the formation of $[GaH_2]^+$ over the formation of Ga^+ (see Text S2). We find that the TS involved in the formation of $[GaH_2]^+$ from $[H-Ga-C_2H_5]^+$ is stabilized considerably by long-range lattice electrostatics in comparison with that associated with the formation of $[GaH_2]^+$ owing to the larger dipole moment associated with the ion-pair TS that forms $[GaH_2]^+$. We note that the use of a long-range corrected approach is critical to predicting this result, as long-range electrostatics provide a more complete picture of TS geometries in zeolites than small cluster approaches.[42,39]

3.5. Summary of Ethane Dehydrogenation Analysis on Ga Species in Ga/H-MFI. On the basis of the summary of the aforementioned results, the only sites found to be both stable and active under reaction conditions for ethane

DOI: 10.1021/acscatal.7b04295
ACS Catal. 2018, 8, 6146−6162

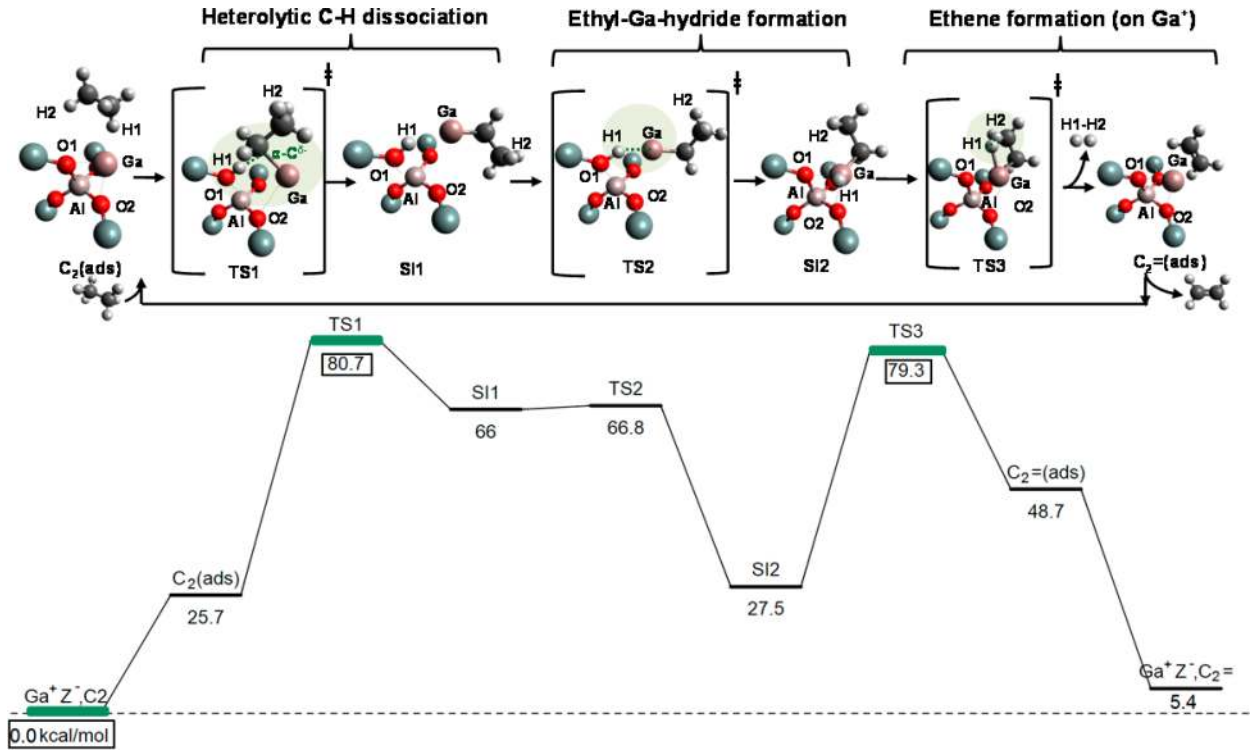

Figure 10. Ethane dehydrogenation via the alkyl mechanism on Ga^+ and the corresponding free energy surface (kcal/mol) reported at 823 K and 1 atm. The free energy span-determining states are labeled in green (with energies in rectangles) as shown by the highest-lying rate-determining transition state (RDTS) and lowest-lying resting state. Only the QM region from the QM/MM model has been displayed here to illustrate the elementary steps in this mechanism.

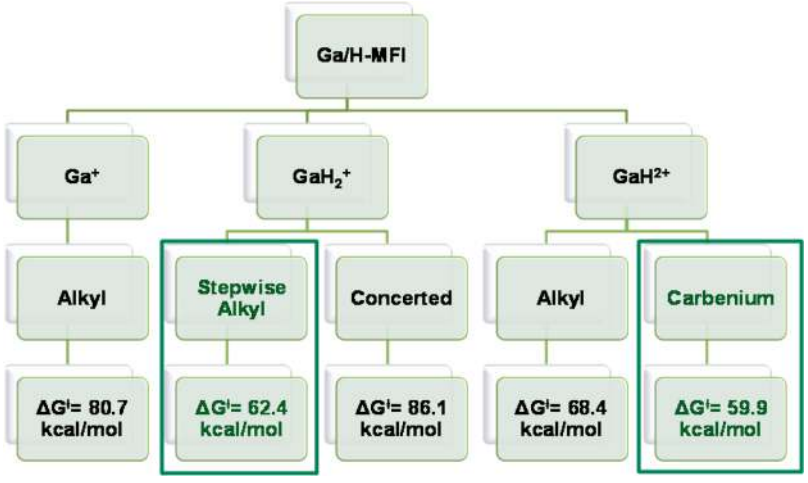

Figure 11. Summary of site and dehydrogenation mechanism analysis on gallium species in Ga/H-MFI based on $\Delta G^{\ddagger}$ (823 K, 1 atm) extracted using the energetic span model for ethane dehydrogenation. Kinetically relevant mechanisms and the sites on which they occur are identified by green boxes.

dehydroaromatization (823 K and 1 atm) are the gallium hydride species: $[GaH_2]^+$ and $[GaH]^{2+}$ in configuration B. Figure 11 summarizes the free energies of activation predicted for 823 K and 1 atm on the basis of the energetic span analysis applied to the free energy surfaces for each of the pathways discussed in sections 3.2−3.4.

Figure 11 indicates that the stepwise alkyl mechanism (identified by the green box) is the favored route for ethane dehydrogenation on $[GaH_2]^+$ for which $\Delta G_{app}^{\ddagger}$ = 62.4 kcal/mol, a value considerably lower than that for the concerted mechanism, 86.1 kcal/mol. Therefore, we conclude that ethane dehydrogenation occurs preferentially on $[GaH_2]^+$ sites via a stepwise alkyl mechanism, rather than a concerted mechanism and, as discussed in section 3.1, this site remains stable under the reaction conditions. For stable $[GaH]^{2+}$ cations in configuration B, the carbenium mechanism ($\Delta G_{app}^{\ddagger}$ = 60.9 kcal/mol) is preferred over the alkyl mechanism ($\Delta G_{app}^{\ddagger}$ = 69.3 kcal/mol) for ethane dehydrogenation. We also note that $[GaH_2]^+$ sites may compete with $[GaH]^{2+}$ sites for ethane dehydrogenation, given that the free energies of activation for both sites are just 2.5 kcal/mol apart, rendering both mechanisms kinetically relevant. Throughout this analysis, we

DOI: 10.1021/acscatal.7b04295
ACS Catal. 2018, 8, 6146−6162

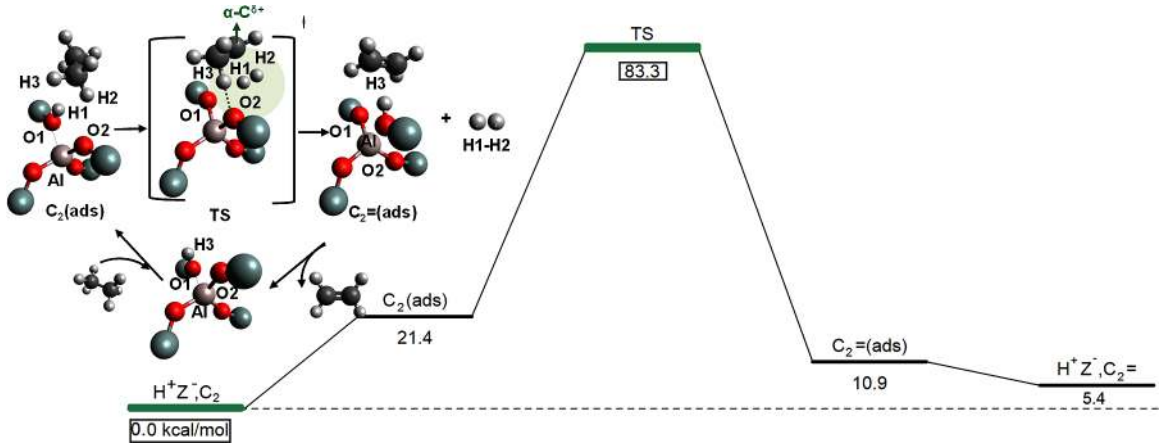

Figure 12. Ethane dehydrogenation via concerted (carbenium) mechanism on H^+ and the corresponding free energy surface (kcal/mol) reported at 823 K and 1 atm. The free energy span-determining states are labeled in green, with energies marked in rectangles, as shown by the highest-lying rate-determining transition state (RDTS) and lowest-lying resting state. Only the QM region from the QM/MM model has been displayed here to illustrate the elementary steps in this mechanism.

have considered alternative mechanisms to be kinetically competitive if their free energy spans are within 4 kcal/mol of each other; however, if the difference is greater than 4 kcal/mol, the more facile mechanism is estimated to proceed with a selectivity of at least 98%,[64−67] and therefore in this case only the more facile mechanism is considered relevant. Finally, we note that the predicted activation enthalpy barriers using our energetic span analysis for ethane dehydrogenation on both $[GaH_2]^+$ ($\Delta H_{app}^{\ddagger}$ = 27.5 kcal/mol) and $[GaH]^{2+}$ ($\Delta H_{app}^{\ddagger}$ = 28.2 kcal/mol) are in good agreement with the experimentally measured barrier of 30.5 kcal/mol.

Whether Ga^+ species exist under the reaction conditions is an open question.[18] However, even if these species do exist under the conditions used for light alkane dehydrogenation over Ga/H-MFI, we show that Ga^+ sites are expected to be less active than $[GaH_2]^+$ sites and participate in light alkane dehydrogenation cycles that end up forming $[GaH_2]^+$ rather than reforming Ga^+ sites (see Text S2). For these reasons, we focus the remainder of the discussion in section 4 on alkane dehydrogenation pathways occurring over $[GaH_2]^+$ and $[GaH]^{2+}$ sites.

4. ROLE OF GALLIUM HYDRIDES IN IMPROVING DEHYDROGENATION IN MFI ZEOLITES

We now extend the theoretical analysis presented in section 3 to the dehydrogenation of C_3 and C_4 alkanes on $[GaH_2]^+$, $[GaH]^{2+}$, and H^+ sites in MFI. In so doing, we also address the question of why the gallium hydride cations in Ga/H-MFI are more active for dehydrogenation than Brønsted acid protons, which occur in both Ga/H-MFI and H-MFI.[68]

Figure 12 illustrates the concerted carbenium mechanism for ethane dehydrogenation on H^+. This process involves the concerted loss of dihydrogen ($H1^+$ and $H2^-$ combination) and the simultaneous formation of a new Brønsted acid site ($H3^+$) at O2.[46] This mechanism has a considerably higher free energy span (of 83.3 kcal/mol) in comparison to the mechanisms found to be kinetically relevant for ethane dehydrogenation on gallium hydrides, discussed in section 3.5; therefore, this pathway is relatively unviable for ethane dehydrogenation under the reaction conditions. Apparent activation enthalpies, predicted via this mechanism for the dehydrogenation of C_2, C_3, n-C_4, and i-C_4 alkanes under the reaction conditions, are given in Table 3. The calculated values are in good agreement with available experimental measurements,[76,77] suggesting that the proposed concerted mechanism can be used to represent the underlying chemistry, as also discussed in our previous work.[45,46]

Table 3. Apparent Enthalpy Barriers ($\Delta H_{app}^{\ddagger}$) for Light Alkane Dehydrogenation (kcal/mol) Predicted Using QM/MM on H^+ Sites in H-MFI in Comparison to Available Experimental Data[a]

light alkane	calcd $\Delta H_{app}^{\ddagger}$ on H^+ (kcal/mol)	measd[76,77] $\Delta H_{app}^{\ddagger}$ for H-MFI (kcal/mol)	Si/Al
ethane	51.2		
propane	48.9	47.8 (±2)	16
butane	46.2	48.3	15
isobutane	46.2		

[a]The range of reported barriers lies between 718 and 823 K.

We now examine the mechanism for the dehydrogenation of C_2, nC_4, and iC_4 alkanes via five mechanisms: (1) the stepwise alkyl mechanism on $[GaH_2]^+$, (2) the alkyl mechanism on $[GaH]^{2+}$, (3) the carbenium mechanism on $[GaH]^{2+}$, (4) the concerted mechanism on $[GaH_2]^+$, and (5) the concerted mechanism on H^+. Since mechanisms 1−3 are not concerted in nature and therefore contain more than a single elementary step (TS), their free energy surfaces are amenable to the energetic span analysis. In sections 3.2−3.3, we found that either the C−H activation or alkene formation steps were the RDTSs on the free energy surfaces for these mechanisms, depending on the mechanism for ethane dehydrogenation. Therefore, for the sake of conciseness, only the predicted free energy spans for both C−H activation and alkene formation are illustrated in Figure 13 for these three multistep mechanisms labeled as (a), (b), and (c). The zero-point corrected energies, enthalpies, and free energy spans for every step in these mechanisms can be found in Tables S1−S23.

Figure 13a shows that the alkyl C−H activation TS is the RDTS for the dehydrogenation of all light alkanes on $[GaH_2]^+$. The same result was observed for ethane dehydrogenation on $[GaH_2]^+$ in section 3.2, and was rationalized on the basis of the high entropic penalty associated with the formation of this TS structure. On the other hand, in Figure 13b, the alkene

DOI: 10.1021/acscatal.7b04295
ACS Catal. 2018, 8, 6146−6162

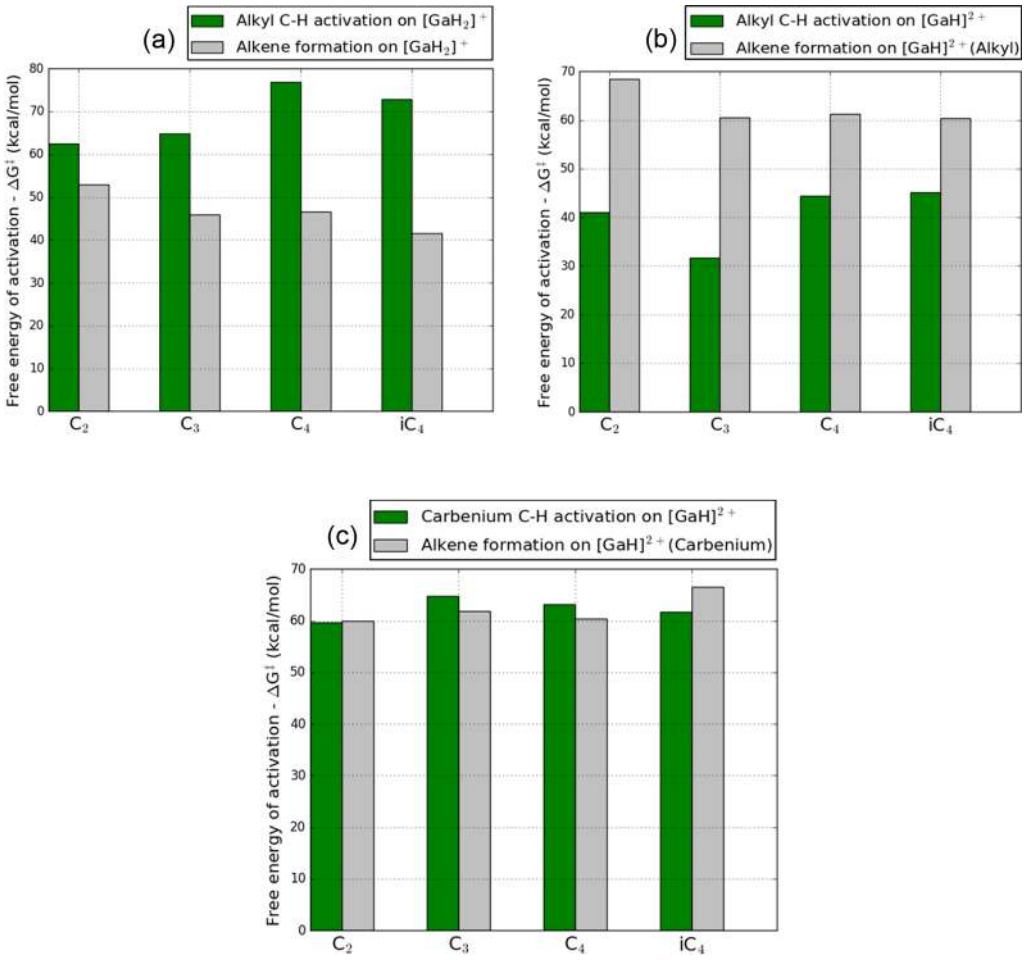

Figure 13. Free energy barriers ($\Delta G^{\ddagger}$) for C−H activation and alkene formation steps on gallium hydrides in Ga/H-MFI under the reaction conditions (823 K and 1 atm). The graphs are reported for (a) stepwise alkyl mechanism on $[GaH_2]^+$, (b) alkyl mechanism on $[GaH]^{2+}$, and (c) carbenium mechanism on $[GaH]^{2+}$. Free energy barriers are obtained from the free energy surfaces of light alkane dehydrogenation mechanisms involving more than one step (see Tables S1−S23). Reported barriers are measured relative to gas-phase light alkanes (lowest-lying resting state for all cases) and are reported in kcal/mol.

formation TS is the RDTS for dehydrogenation of all light alkanes via the alkyl mechanism on $[GaH]^{2+}$. This observation is similar to that for ethane dehydrogenation reported in section 3.3, where the formation of alkenes from more stable alkyl intermediate structures is kinetically limiting. Finally for the carbenium mechanism on $[GaH]^{2+}$ shown in Figure 13c, C−H activation and alkene formation can compete with each other as RDTSs. This observation is once again similar to that for ethane dehydrogenation discussed in section 3.3. The natures of the RDTSs associated with all these three mechanisms are summarized in Table 4.

The free energies of activation for the aforementioned mechanisms (containing multiple steps, predicted using the energetic span model) are reported together with those for the other concerted mechanisms in Figure 14, alongside their corresponding enthalpies of activation under the reaction conditions. As seen in Figure 14, the mechanism with the lowest enthalpy of activation is generally seen to also have the lowest free energy of activation (free energy span). Therefore, enthalpic effects in these light alkane dehydrogenation mechanisms play an important role in explaining the differences in activities for different mechanisms.

Comparison of the values of $\Delta G^{\ddagger}$ and $\Delta H^{\ddagger}$ in Figure 14 allows one to determine entropic contributions $-T\Delta S^{\ddagger}$ to $\Delta G^{\ddagger}$ and to establish the relative importance of these contributions to the value of $\Delta G^{\ddagger}$ for all investigated mechanisms. As the relative $\Delta G^{\ddagger}$ and $\Delta H^{\ddagger}$ values on the two graphs are similar, relative $-T\Delta S^{\ddagger}$ contributions between different mechanisms

Table 4. Nature of Rate-Determining Transition State (RDTS) Obtained from Energetic Span Analysis of Free Energy Surfaces for Dehydrogenation of Light Alkanes (Ethane, Propane, Butane, and Isobutane) on Gallium Hydrides[a]

alkane	stepwise alkyl/ $[GaH_2]^+$	alkyl/ $[GaH]^{2+}$	carbenium/$[GaH]^{2+}$
ethane	C−H activation	ethene formation	ethene formation, C−H activation
propane	C−H activation	propene formation	propene formation, C−H activation
butane	C−H activation	butene formation	butene formation, C−H activation
isobutane	C−H activation	isobutene formation	isobutene formation

[a]See Tables S1−S23 for all the zero-point corrected enthalpy and free energy surfaces for these mechanisms computed at 823 K and 1 atm. The alkane C−H activation step is associated with the first C−H cleavage (α-C), while the alkene formation step is associated with the second C−H cleavage (β-C).

DOI: 10.1021/acscatal.7b04295
ACS Catal. 2018, 8, 6146−6162

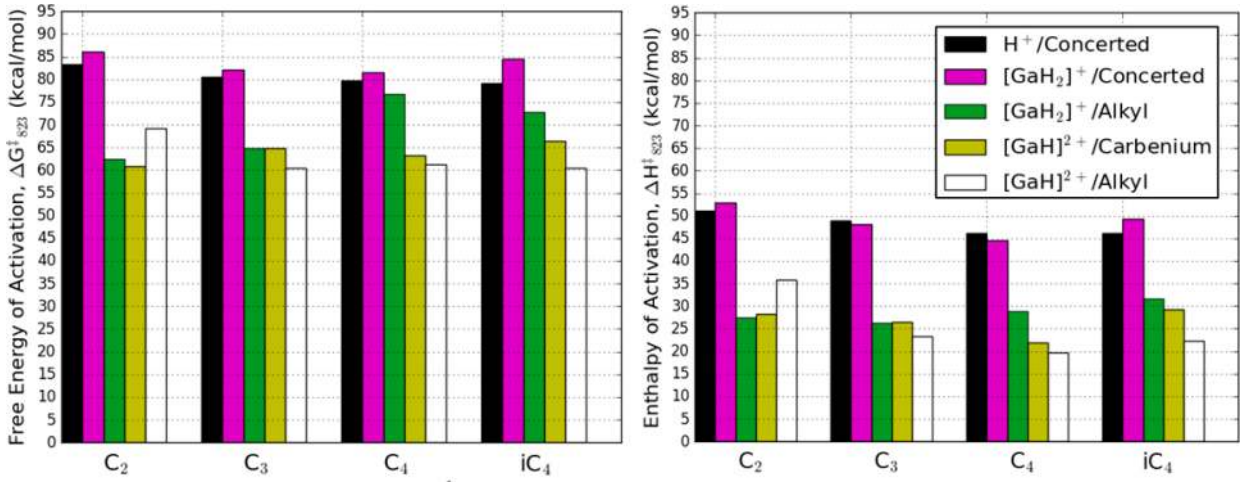

Figure 14. Free energy spans ($\Delta G^{\ddagger}$) for light alkane dehydrogenation (kcal/mol) predicted using QM/MM for H^+- and Ga-based sites under the reaction conditions (823 K and 1 atm). All barriers were calculated by applying the energetic span model to the free energy surface of each mechanism. For mechanisms involving more than one step, the RDTS is either the C−H activation or alkene formation step, depending on the mechanism of interest (see Table 4).

Table 5. Apparent Enthalpy Barriers ($\Delta H_{app}^{\ddagger}$) for Light Alkane Dehydrogenation (kcal/mol) Predicted Using QM/MM on Ga-Based Sites in Comparison to Available Experimental Data Measured for Light Alkane Dehydrogenation on Ga/H-MFI[a]

	calcd $\Delta H_{app}^{\ddagger}$ (kcal/mol)			measd $\Delta H_{app}^{\ddagger}$ (kcal/mol)[28,82,83]		
light alkane	$[GaH_2]^+$ (stepwise alkyl)	$[GaH]^{2+}$ (carbenium)	$[GaH]^{2+}$ (alkyl)	Ga/H-MFI	Ga/Al	Si/Al
ethane	**27.5**	**28.2**	35.8	30.5	0.5	16
propane	26.2	26.5	**23.4**	25.6	0.4	16
butane	28.9	**21.9**	**19.8**			
isobutane	31.7	29.3	**22.3**	23.8	0.1	16.5

[a]The range of reported barriers is based on measurements made between 718 and 823 K. The activation barriers reported in boldface are found to be kinetically relevant on the basis of our energetic span analysis.

appear to be similar. The exception to this trend is the stepwise alkyl mechanism for the dehydrogenation of larger alkanes (iC_4 and nC_4). The entropic penalty for the RDTS in this mechanism increases considerably with increasing chain length, in comparison to other mechanisms. This effect is evident in Figure 14: for ethane dehydrogenation, the free energy barriers for the (stepwise) alkyl mechanism on $[GaH_2]^+$ and the carbenium mechanism on $[GaH]^{2+}$ are within 4 kcal/mol of each other. Therefore, these two mechanisms for ethane dehydrogenation are expected to compete with each other (as also concluded in section 3.5). However, with increasing alkane chain length, the alkyl mechanism on $[GaH_2]^+$ gives rise to higher free energy barriers, relative to other mechanisms on $[GaH]^{2+}$. This result is attributed to the observed importance of entropic effects for the RDTS in the stepwise alkyl mechanism on $[GaH_2]^+$, as discussed in section 3.2. The motion of the alkyl fragment in this RDTS complex is severely limited, as this fragment is strongly bound to both Ga and H^+ moieties on the zeolite surface. Since the entropic penalty for this RDTS increases with chain length and leads to higher free energies of activation relative to other pathways, the (stepwise) alkyl mechanism on $[GaH_2]^+$ becomes uncompetitive for dehydrogenation of alkanes larger than ethane.

We further observe in Figure 14 that the free energies of activation calculated on both gallium hydrides via alkyl and carbenium pathways are considerably lower than those calculated for the concerted mechanism on H^+. This finding agrees qualitatively with experimental observations, which report higher rates of light alkane dehydrogenation over Ga/H-MFI in comparison to H-MFI.[6] We also note that the concerted mechanism on $[GaH_2]^+$ is once again found to be kinetically uncompetitive for all light alkanes due to reasons already discussed in section 3.2. Figure 14 also illustrates that, with the exception of ethane dehydrogenation, light alkane dehydrogenation occurs preferentially on $[GaH]^{2+}$ via the alkyl mechanism. This finding is consistent with the observation of metal−alkyl species during the interactions of small alkanes with high-silica zeolites modified with Ga (or Zn) on the basis of ^{13}C MAS NMR, DRIFTS, and other spectroscopic techniques reported by Stepanov and co-workers.[78−81]

We also note that the observed high activity of $[GaH]^{2+}$ is consistent with the proposal by Bhan and co-workers based on microkinetic studies of propane aromatization and FT-IR that $[GaH]^{2+}$ sites are the most active form of reduced Ga species for dehydrogenation in Ga/H-MFI, especially at Ga/Al ratios ≤0.5.[32] Table 5 compares the calculated activation enthalpies for the dehydrogenation of C_2 through C_4 alkanes on gallium hydrides for favored mechanisms predicted on the basis of the energetic span analysis. Our predictions are compared with experimentally measured activation barriers for alkane dehydrogenation over Ga/H-MFI conducted under conditions of differential conversion or after correction for secondary reactions.[28,82,83] The activation barriers predicted for mechanisms identified to be kinetically relevant on the basis of our energetic span analysis are marked in boldface. As the carbenium mechanism is also found to compete with the alkyl mechanism for butane dehydrogenation, two activation enthalpy barrier heights are predicted for butane dehydrogen-

DOI: 10.1021/acscatal.7b04295
ACS Catal. 2018, 8, 6146−6162

ation on $[GaH]^{2+}$. Good agreement is observed between the calculated barriers and the available experimental data.

Taken together, the results in Figure 14 and the description of mechanisms reported in sections 3.2 and 3.3 suggest that, although Lewis acidic gallium hydrides ($[GaH]^{2+}$ and $[GaH_2]^{+}$) are structurally different, both are able to provide considerable electronic stabilization to C−H cleavage TSs. This could occur either directly via interaction of C with the gallium center (e.g., $C^{\delta-}-Ga^{\delta+}$ in the alkyl mechanisms) or via the interaction with framework oxygen atoms of the zeolite (as $C^{\delta+}-O^{\delta-}$ in the carbenium mechanisms), leading to favorable enthalpic (electronic) and free energies of activation for the dissociation of σ-C−H bonds on gallium hydrides. This type of electronic stabilization does not occur when dehydrogenation is catalyzed by Brønsted acid protons, resulting in considerably higher electronic and enthalpic and subsequently free energy barriers for light alkane dehydrogenation in comparison to those observed on gallium hydrides. As cleaving the unreactive C−H bond is considered the energetic bottleneck in the activation of small alkanes,[84] we propose on the basis of our analysis that gallium hydrides in Ga/H-MFI play a critical role in facilitating C−H bond cleavage via both alkyl and carbenium mechanisms.

Finally, we observe in Figure 13 that the alkyl mechanism on $[GaH]^{2+}$ becomes more favorable (i.e., lower free energies) with increasing alkane chain length, more so than the carbenium pathway, especially for propane, butane, and isobutane dehydrogenation. This observed trend of lower free energy barriers of the alkyl mechanism on $[GaH]^{2+}$ with increasing chain length can be explained by examining the electronic structure of the RDTS. This RDTS is illustrated in Figure 14 and represents the alkene formation step. The β-Cs in these TSs are mildly carbenium like in character in comparison to the α-Cs, which are bonded to the gallium center and are carbanion-like (see Figure S1). Figure 15 shows that the activation enthalpy for ethane vs propane dehydrogenation decreases from 35.8 to 23.4 kcal/mol. This decrease is attributable to the electrostatic induction effect associated with the additional methyl group to the β-C. On the other hand, a smaller decrease in the activation enthalpy is observed on progressing from propane to the butane dehydrogenation: 23.4 to 19.8 kcal/mol. The smaller change is due to the location of the electron-donating group one backbone carbon away from the β-C. In contrast, the activation enthalpy for isobutane dehydrogenation is higher than that for butane dehydrogenation: 22.3 vs 19.3 kcal/mol. In this case, the inductive effect of the additional methyl group adjacent to the β-C may be offset by a steric hindrance associated with the TS for isobutene formation requiring a tertiary C to orient itself for the formation of dihydrogen and isobutene in the tight space around the available proton, with which it interacts. However, since the gain in activation entropy is nevertheless favorable for the isobutene formation TS due to the release of both dihydrogen and alkene, the alkyl mechanism on $[GaH]^{2+}$ nevertheless remains the most favorable dehydrogenation pathway, even for iC_4 dehydrogenation.

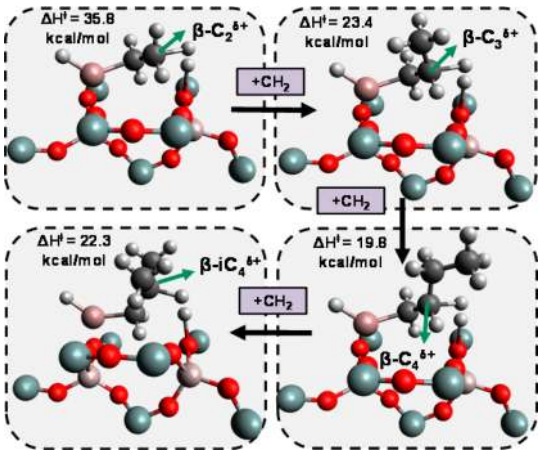

Figure 15. Illustration of the effect of increasing chain length and substitution on light alkene formation TSs in the alkyl light alkane dehydrogenation mechanism on $[GaH]^{2+}$. Only the QM region from the QM/MM model has been displayed here for illustration purposes. The green arrow indicates the β-C on a particular light alkene formation TS.

5. CONCLUSIONS

We have investigated the relative stability of several reduced Ga cationic species and their activities for the dehydrogenation of light alkanes. This effort has involved an examination of the free energy landscape for all processes and has used energetic span analyses to identify the rate-determining TS for each reaction process. Electronic structure calculations were carried out with a quantum mechanics/molecular mechanics model that uses a range-separated hybrid density functional and accounts for dispersive interactions, together with a high-order basis set. The molecular mechanics portion of these calculations involves parameters chosen to capture experimentally measured heats of adsorption for a wide variety of adsorbates (polar and nonpolar) in different zeolites. Our analysis has revealed that univalent and divalent gallium hydrides, $[GaH_2]^{+}$ and $[GaH]^{2+}$ respectively, are more active for dehydrogenation in comparison to H^{+} sites and thermodynamically stable Ga^{+} sites. Overall, $[GaH]^{2+}$ is found to be the most active site for light alkane dehydrogenation. The TS for this site provides enthalpic stabilization for C−H cleavage via alkyl and carbenium dehydrogenation pathways. In contrast, the TS for carbenium-like C−H cleavage on Brønsted acid sites is found to be less enthalpically favored due to the limited electronic interactions of this TS with the atoms in the framework and the proton. Activation barriers predicted under the reaction conditions for light alkane dehydrogenation are in good agreement with available experimental data which have been measured for alkane to alkene dehydrogenation in H-MFI and Ga/H-MFI. With increasing length of the alkane, we find that constrained TSs can become less favorable due to increasing entropic penalties relative to the gas-phase alkanes. We also observe that the alkyl mechanism becomes more favorable with increasing chain length because of the enthalpic favorability of the TS responsible for the second C−H cleavage step leading to light alkene formation.

6. ADDITIONAL NOTE

During the resubmission of our manuscript, a paper appeared dealing with the dehydrogenation of light alkanes over Ga/H-MFI.[85] In this study, the catalytically active site is taken to be a Ga^{+} cation coordinated with one charge-exchange site and a proton on an NNN charge-exchange site. The authors of this paper analyze the Gibbs free energy and enthalpy landscapes on which the dehydrogenation of propane occurs. DFT calculations were carried out for a periodic model of the zeolite using a dispersion-corrected PBE functional and a plane-wave basis

DOI: 10.1021/acscatal.7b04295
ACS Catal. 2018, 8, 6146−6162

set. The authors also propose that $[GaH]^{2+}$ sites can reduce to form a pair of Ga^+ and H^+ sites; however, the saddle point for this process was not defined nor was the role of Al−Al distances[21,25] on the stability of $[GaH]^{2+}$ considered.

We have used our energetic span model to analyze the free energy surface presented in this study for the dehydrogenation of propane, so as to compare these results with the findings that are reported in our work. We estimate the free energy spans for the two steps that are found to compete with each other as the RDTSs for propane dehydrogenation at 783 K—C−H cleavage and H_2 elimination—have almost identical free energy spans, $\Delta G^{\ddagger} \approx 78$ kcal/mol. The aforementioned value is smaller than the free energy span predicted using our model for propane dehydrogenation on Ga^+ ($\Delta G^{\ddagger} \approx 85$ kcal/mol) under the authors' stated reference conditions; nonetheless, this aforementioned value of $\Delta G^{\ddagger}$ is much higher than those for $[GaH]^{2+}$ and $[GaH_2]^+$ discussed in the present study ($\Delta G^{\ddagger} \approx$ 67 and 72 kcal/mol, respectively). We also note that this aforementioned estimate of the free energy span for propane dehydrogenation predicted in the new study is much higher than that which would be predicted by considering $[GaH]^{2+}$ as the resting state on the free energy surface, found by the authors of ref 85, $\Delta G^{\ddagger} \approx 56$ kcal/mol Furthermore, the possibility of $[GaH_2]^+$ formation at the end of the catalytic cycle was not considered in the newly published study. This is a significant consideration, because we have demonstrated in Text S2 that the free energy barriers responsible for the formation of gallium hydrides from alkyl Ga hydride intermediates are kinetically favored over those of univalent Ga species. Therefore, we propose that Ga^+ sites, which may be thermodynamically stable in Ga/H-MFI, are less likely to catalyze C−H cleavage steps as effectively as $[GaH]^{2+}$ sites and are more likely to form kinetically favored $[GaH_2]^+$ sites under the reaction conditions.

■ ASSOCIATED CONTENT

Supporting Information

The Supporting Information is available free of charge on the ACS Publications website at DOI: 10.1021/acscatal.7b04295.

Electronic, enthalpic, and free energy calculations reported for all the reaction mechanisms investigated in this work, other detailed calculations, including application of the energetic span analysis on less stable $[GaH]^{2+}$ cations, and calculations on the conversion of alkyl Ga hydride intermediates into alkenes on Ga^+ and $[GaH_2]^+$ sites and the energy spans for C−H cleavage steps on Ga^+ sites (PDF)

■ AUTHOR INFORMATION

Corresponding Author

*E-mail for A.T.B.: alexbell@berkeley.edu.

ORCID

Martin Head-Gordon: 0000-0002-4309-6669

Alexis T. Bell: 0000-0002-5738-4645

Notes

The authors declare no competing financial interest.

■ ACKNOWLEDGMENTS

This work was supported by a grant from Chevron Energy Technology Co. We are also thankful to UC Berkeley's Molecular Graphics and Computation Facility (supported by NIH S10OD023532) for providing computational resources. E.M. gratefully acknowledges financial support from the Abu Dhabi National Oil Company (ADNOC) through a Ph.D. Fellowship. E.M. also thanks colleagues (external affiliation) Dr. Yi-Pei Li (Massachusetts Institute of Technology), Neelay Phadke and Dr. Jeroen Van der Mynsbrugge (Ghent University), Matthieu Bondil (École Polytechnique Fédérale de Lausanne), and Dr. James Paul Dombrowski (Northwestern University) for enlightening discussions about modeling light alkane catalysis on zeolites and other physicochemical properties of gallium compounds.

■ REFERENCES

(1) Franck, H.-G.; Stadelhofer, J. W. *Industrial Aromatic Chemistry*, 1st ed.; Springer-Verlag: Frankfurt, Germany, 1989; pp 1−499.

(2) Al-Zahrani, S. M. Catalytic Conversion of LPG to High-Value Aromatics: The Current State of the Art and Future Predictions. *Dev. Chem. Eng. Miner. Process.* **1998**, *6*, 101−120.

(3) Glaser, R.; Weitkamp, J. The Application of Zeolites in Catalysis. *Springer Ser. Chem. Phys.* **2004**, *75*, 159−212.

(4) Narbeshuber, T. F.; Vinek, H.; Lercher, J. A. Monomolecular Conversion of Light Alkanes over H-ZSM-5. *J. Catal.* **1995**, *157*, 388−395.

(5) Bhan, A.; Nicholas Delgass, W. Propane Aromatization over HZSM-5 and Ga/HZSM-5 Catalysts. *Catal. Rev.: Sci. Eng.* **2008**, *50*, 19−151.

(6) Ono, Y. Transformation of Lower Alkanes Into Aromatic-Hydrocarbons Over Zsm-5 Zeolites. *Catal. Rev.: Sci. Eng.* **1992**, *34*, 179−226.

(7) Hagen, A.; Roessner, F. Ethane to Aromatic Hydrocarbons: Past, Present, Future. *Catal. Rev.: Sci. Eng.* **2000**, *42*, 403−437.

(8) Guisnet, M.; Gilson, J.-P. *Zeolites for Cleaner Technologies*; Imperial College Press: London, 2002; pp 1−390.

(9) Guisnet, M.; Gnep, N. S. Aromatization of Propane over GaHMFI Catalysts. Reaction Scheme, Nature of the Dehydrogenating Species and Mode of Coke Formation. *Catal. Today* **1996**, *31*, 275−292.

(10) Lukyanov, D. B.; Gnep, N. S.; Guisnet, M. R. Kinetic Modeling of Propane Aromatization Reaction over HZSM-5 and GaHZSM-5. *Ind. Eng. Chem. Res.* **1995**, *34*, 516−523.

(11) Meitzner, G. D.; Iglesia, E.; Baumgartner, J. E.; Huang, E. S. The Chemical State of Gallium in Working Alkane Dehydrocyclodimerization Catalysts. In Situ Gallium K-Edge X-Ray Absorption Spectroscopy. *J. Catal.* **1993**, *140*, 209−225.

(12) Kazansky, V. B.; Subbotina, I. R.; Rane, N.; van Santen, R. A.; Hensen, E. J. M. On Two Alternative Mechanisms of Ethane Activation over ZSM-5 Zeolite Modified by Zn2+ and Ga1+ Cations. *Phys. Chem. Chem. Phys.* **2005**, *7*, 3088−3092.

(13) Kazansky, V. B.; Subbotina, I. R.; Van Santen, R. A.; Hensen, E. J. M. DRIFTS Study of the Chemical State of Modifying Gallium Ions in Reduced Ga/ZSM-5 Prepared by Impregnation. I. Observation of Gallium Hydrides and Application of CO Adsorption as Molecular Probe for Reduced Gallium Ions. *J. Catal.* **2004**, *227*, 263−269.

(14) Faro, A. d. C.; Oliveira, V. D. Pulse Reaction Studies of Gallium Modified H-ZSM5 Catalysts with Propane. *Stud. Surf. Sci. Catal.* **2008**, *174*, 1155−1158.

(15) Rodrigues, V. d. O.; Eon, J. G.; Faro, A. C. Correlations between Dispersion, Acidity, Reducibility, and Propane Aromatization Activity of Gallium Species Supported on HZSM5 Zeolites. *J. Phys. Chem. C* **2010**, *114*, 4557−4567.

(16) Rane, N.; Overweg, A. R.; Kazansky, V. B.; van Santen, R. A.; Hensen, E. J. M. Characterization and Reactivity of Ga+ and GaO+ Cations in Zeolite ZSM-5. *J. Catal.* **2006**, *239*, 478−485.

(17) Meitzner, G. D.; Iglesia, E.; Baumgartner, J. E.; Huang, E. S. The Chemical State of Gallium in Working Alkane Dehydrocyclodimerization Catalysts. In Situ Gallium K-Edge X-Ray Absorption Spectroscopy. *J. Catal.* **1993**, *140*, 209−225.

DOI: 10.1021/acscatal.7b04295
ACS Catal. 2018, 8, 6146−6162

(18) Getsoian, A. B.; Das, U.; Camacho-Bunquin, J.; Zhang, G.; Gallagher, J. R.; Hu, B.; Cheah, S.; Schaidle, J. A.; Ruddy, D. A.; Hensley, J. E.; et al. Organometallic Model Complexes Elucidate the Active Gallium Species in Alkane Dehydrogenation Catalysts Based on Ligand Effects in Ga K-Edge XANES. *Catal. Sci. Technol.* **2016**, *6*, 6339−6353.
(19) Pidko, E. A.; Kazansky, V. B.; Hensen, E. J. M.; van Santen, R. A. A Comprehensive Density Functional Theory Study of Ethane Dehydrogenation over Reduced Extra-Framework Gallium Species in ZSM-5 Zeolite. *J. Catal.* **2006**, *240*, 73−84.
(20) Milas, I.; Nascimento, M. A. C. A Density Functional Study on the Effect of the Zeolite Cavity on Its Catalytic Activity: The Dehydrogenation and Cracking Reactions of Isobutane over HZSM-5 and HY Zeolites. *Chem. Phys. Lett.* **2006**, *418*, 368−372.
(21) Joshi, Y. V.; Thomson, K. T. High Ethane Dehydrogenation Activity of [GaH]2+ Al Pair Sites in Ga/H-[Al]ZSM-5: A DFT Thermochemical Analysis of the Catalytic Sites under Reaction Conditions. *J. Catal.* **2007**, *246*, 249−265.
(22) Pidko, E. a.; Hensen, E. J. M.; van Santen, R. a. Dehydrogenation of Light Alkanes over Isolated Gallyl Ions in Ga/ZSM-5 Zeolites. *J. Phys. Chem. C* **2007**, *111*, 13068−13075.
(23) Kuz'min, I. V.; Zhidomirov, G. M.; Solkan, V. N.; Kazanskii, V. B. Quantum Chemical Calculation of the Catalytic Reaction of Ethane Dehydrogenation on Gallium Oxide-Hydroxide Binuclear Clusters in Oxidized GaO/ZSM-5 Zeolite. *Kinet. Catal.* **2009**, *50*, 752−759.
(24) Zhidomirov, G. M.; Shubin, A. A.; Milov, M. A.; Kazansky, V. B.; Van Santen, R. A.; Hensen, E. J. M. Cluster Model DFT Study of CO Adsorption to Gallium Ions in Ga/HZSM-5. *J. Phys. Chem. C* **2008**, *112*, 3321−3326.
(25) Joshi, Y. V.; Thomson, K. T. The Roles of Gallium Hydride and Brønsted Acidity in Light Alkane Dehydrogenation Mechanisms Using Ga-Exchanged HZSM-5 Catalysts: A DFT Pathway Analysis. *Catal. Today* **2005**, *105*, 106−121.
(26) Pereira, M. S.; Da Silva, A. M.; Nascimento, M. A. C. Effect of the Zeolite Cavity on the Mechanism of Dehydrogenation of Light Alkanes over Gallium-Containing Zeolites. *J. Phys. Chem. C* **2011**, *115*, 10104−10113.
(27) Pereira, M. S.; Nascimento, M. A. C. Theoretical Study on the Dehydrogenation Reaction of Alkanes Catalyzed by Zeolites Containing Nonframework Gallium Species. *J. Phys. Chem. B* **2006**, *110*, 3231−3238.
(28) Bandiera, J.; Taârit, Y. B. Ethane Conversion: Kinetic Evidence for the Competition of Consecutive Steps for the Same Active Centre. *Appl. Catal., A* **1997**, *152*, 43−51.
(29) Solkan, V. N.; Zhidomirov, G. M.; Kazansky, V. B. Density Functional Theory Studies of Nitrous Oxide Adsorption and Decomposition on Ga-ZSM-5. *Int. J. Quantum Chem.* **2007**, *107*, 2417−2425.
(30) Hensen, E. J. M.; Pidko, E. A.; Rane, N.; Van Santen, R. A. Water-Promoted Hydrocarbon Activation Catalyzed by Binuclear Gallium Sites in ZSM-5 Zeolite. *Angew. Chem., Int. Ed.* **2007**, *46*, 7273−7276.
(31) Dooley, K. M.; Chang, C.; Price, G. L. Effects of Pretreatments on State of Gallium and Aromatization Activity of gallium/ZSM-5 Catalysts. *Appl. Catal., A* **1992**, *84*, 17−30.
(32) Krishnamurthy, G.; Bhan, A.; Delgass, W. N. Identity and Chemical Function of Gallium Species Inferred from Microkinetic Modeling Studies of Propane Aromatization over Ga/HZSM-5 Catalysts. *J. Catal.* **2010**, *271*, 370−385.
(33) Pidko, E. A.; Van Santen, R. A. Structure-Reactivity Relationship for Catalytic Activity of Gallium Oxide and Sulfide Clusters in Zeolite. *J. Phys. Chem. C* **2009**, *113*, 4246−4249.
(34) Pidko, E. A.; Hensen, E. J. M.; van Santen, R. A. Self-Organization of Extraframework Cations in Zeolites. *Proc. R. Soc. London, Ser. A* **2012**, *468*, 2070−2086.
(35) Pidko, E. A.; Hensen, E. J. M.; Zhidomirov, G. M.; van Santen, R. A. Non-Localized Charge Compensation in Zeolites: A Periodic DFT Study of Cationic Gallium-Oxide Clusters in Mordenite. *J. Catal.* **2008**, *255*, 139−143.
(36) Pidko, E. A.; van Santen, R. A.; Hensen, E. J. M. Multinuclear Gallium-Oxide Cations in High-Silica Zeolites. *Phys. Chem. Chem. Phys.* **2009**, *11*, 2893−2902.
(37) Kuźmin, I. V.; Sokolova, N. A.; Subbotina, I. R.; Zhidomirov, G. M. Ethylene Adsorption and Transformation on Zeolite Ga+/ZSM-5. *Russ. Chem. Bull.* **2015**, *64*, 278−283.
(38) Subbotina, I. R.; Sokolova, N. A.; Kuz'min, I. V.; Zhidomirov, G. M.; Kazanskii, V. B. Adsorption Properties of Oxidized Gallium-Modified Zeolite ZSM-5 from Diffuse Reflectance IR and Quantum-Chemical Data: 1. Interaction with Hydrogen and Ethane. *Kinet. Catal.* **2007**, *48*, 735−741.
(39) Zygmunt, S. A.; Curtiss, L. A.; Zapol, P.; Iton, L. E. Ab Initio and Density Functional Study of the Activation Barrier for Ethane Cracking in Cluster Models of Zeolite H-ZSM-5. *J. Phys. Chem. B* **2000**, *104*, 1944−1949.
(40) Vollmer, J. M.; Truong, T. N. Mechanisms of Hydrogen Exchange of Methane with H-Zeolite Y: An Ab Initio Embedded Cluster Study. *J. Phys. Chem. B* **2000**, *104*, 6308−6312.
(41) Hansen, N.; Brüggemann, T.; Krishna, R.; Van Baten, J. M.; Keil, F. J.; Bell, A. T. Alkylation of Benzene with Ethene over H-ZSM-5-A Multiscale Investigation. *J. Phys. Chem. C* **2008**, *112*, 15402−15411.
(42) Mansoor, E.; Van der Mynsbrugge, J.; Head-Gordon, M.; Bell, A. T. Impact of Long-Range Electrostatic and Dispersive Interactions on Theoretical Predictions of Adsorption and Catalysis in Zeolites. *Catal. Today* **2018**, 1−15.
(43) Gounder, R.; Iglesia, E. The Roles of Entropy and Enthalpy in Stabilizing Ion-Pairs at Transition States in Zeolite Acid Catalysis. *Acc. Chem. Res.* **2012**, *45*, 229−238.
(44) Li, Y.-P.; Gomes, J.; Mallikarjun Sharada, S.; Bell, A. T.; Head-Gordon, M. Improved Force-Field Parameters for QM/MM Simulations of the Energies of Adsorption for Molecules in Zeolites and a Free Rotor Correction to the Rigid Rotor Harmonic Oscillator Model for Adsorption Enthalpies. *J. Phys. Chem. C* **2015**, *119*, 1840−1850.
(45) Van der Mynsbrugge, J.; Janda, A.; Mallikarjun Sharada, S.; Lin, L.-C.; Van Speybroeck, V.; Head-Gordon, M.; Bell, A. T. Theoretical Analysis of the Influence of Pore Geometry on Monomolecular Cracking and Dehydrogenation of N-Butane in Brønsted-Acid Zeolites. *ACS Catal.* **2017**, *7*, 2685−2697.
(46) Mallikarjun Sharada, S.; Zimmerman, P. M.; Bell, A. T.; Head-Gordon, M. Insights into the Kinetics of Cracking and Dehydrogenation Reactions of Light Alkanes in H-MFI. *J. Phys. Chem. C* **2013**, *117*, 12600−12611.
(47) Zimmerman, P. M.; Head-Gordon, M.; Bell, A. T. Selection and Validation of Charge and Lennard-Jones Parameters for QM/MM Simulations of Hydrocarbon Interactions with Zeolites. *J. Chem. Theory Comput.* **2011**, *7*, 1695−1703.
(48) Li, Y. P.; Head-Gordon, M.; Bell, A. T. Computational Study of P -Xylene Synthesis from Ethylene and 2,5-Dimethylfuran Catalyzed by H-BEA. *J. Phys. Chem. C* **2014**, *118*, 22090−22095.
(49) Olson, D. H.; Khosrovani, N.; Peters, A. W.; Toby, B. H. Crystal Structure of Dehydrated CsZSM-5 (5.8Al): Evidence for Nonrandom Aluminum Distribution. *J. Phys. Chem. B* **2000**, *104*, 4844−4848.
(50) Gomes, J.; Zimmerman, P. M.; Head-Gordon, M.; Bell, A. T. Accurate Prediction of Hydrocarbon Interactions with Zeolites Utilizing Improved Exchange-Correlation Functionals and QM/MM Methods: Benchmark Calculations of Adsorption Enthalpies and Application to Ethene Methylation by Methanol. *J. Phys. Chem. C* **2012**, *116*, 15406−15414.
(51) Shao, Y.; Molnar, L. F.; Jung, Y.; Kussmann, J.; Ochsenfeld, C.; Brown, S. T.; Gilbert, A. T. B.; Slipchenko, L. V.; Levchenko, S. V.; O'Neill, D. P.; et al. Advances in Methods and Algorithms in a Modern Quantum Chemistry Program Package. *Phys. Chem. Chem. Phys.* **2006**, *8*, 3172−3191.
(52) Behn, A.; Zimmerman, P. M.; Bell, A. T.; Head-Gordon, M. Efficient Exploration of Reaction Paths via a Freezing String Method. *J. Chem. Phys.* **2011**, *135*, 224108.

DOI: 10.1021/acscatal.7b04295
ACS Catal. 2018, 8, 6146−6162

(53) Chai, J.-D.; Head-Gordon, M. Long-Range Corrected Hybrid Density Functionals with Damped Atom−atom Dispersion Corrections. *Phys. Chem. Chem. Phys.* **2008**, *10*, 6615.
(54) Mardirossian, N.; Head-Gordon, M. Thirty Years of Density Functional Theory in Computational Chemistry: An Overview and Extensive Assessment of 200 Density Functionals. *Mol. Phys.* **2017**, *115*, 2315−2372.
(55) Goerigk, L.; Hansen, A.; Bauer, C. A.; Ehrlich, S.; Najibi, A.; Grimme, S. A Look at the Density Functional Theory Zoo with the Advanced GMTKN55 Database for General Main Group Thermochemistry, Kinetics and Noncovalent Interactions. *Phys. Chem. Chem. Phys.* **2017**, *19*, 32184−32215.
(56) Li, Y. P.; Head-Gordon, M.; Bell, A. T. Theoretical Study of 4-(Hydroxymethyl)benzoic Acid Synthesis from Ethylene and 5-(Hydroxymethyl)furoic Acid Catalyzed by Sn-BEA. *ACS Catal.* **2016**, *6*, 5052−5061.
(57) Li, Y. P.; Head-Gordon, M.; Bell, A. T. Analysis of the Reaction Mechanism and Catalytic Activity of Metal-Substituted Beta Zeolite for the Isomerization of Glucose to Fructose. *ACS Catal.* **2014**, *4*, 1537−1545.
(58) Weinhold, F.; Landis, C. R. Natural Bond Orbitals and Extensions of Localized Bonding Concepts. *Chem. Educ. Res. Pract.* **2001**, *2*, 91−104.
(59) Shao, Y.; Gan, Z.; Epifanovsky, E.; Gilbert, A. T. B.; Wormit, M.; Kussmann, J.; Lange, A. W.; Behn, A.; Deng, J.; Feng, X.; et al. Advances in Molecular Quantum Chemistry Contained in the Q-Chem 4 Program Package. *Mol. Phys.* **2015**, *113*, 184−215.
(60) De Moor, B. A.; Ghysels, A.; Reyniers, M. F.; Van Speybroeck, V.; Waroquier, M.; Marin, G. B. Normal Mode Analysis in Zeolites: Toward an Efficient Calculation of Adsorption Entropies. *J. Chem. Theory Comput.* **2011**, *7*, 1090−1101.
(61) Piccini, G.; Sauer, J. Quantum Chemical Free Energies: Structure Optimization and Vibrational Frequencies in Normal Modes. *J. Chem. Theory Comput.* **2013**, *9*, 5038−5045.
(62) Grimme, S. Supramolecular Binding Thermodynamics by Dispersion-Corrected Density Functional Theory. *Chem. - Eur. J.* **2012**, *18*, 9955−9964.
(63) Janda, A.; Vlaisavljevich, B.; Lin, L. C.; Mallikarjun Sharada, S.; Smit, B.; Head-Gordon, M.; Bell, A. T. Adsorption Thermodynamics and Intrinsic Activation Parameters for Monomolecular Cracking of N-Alkanes on Brønsted Acid Sites in Zeolites. *J. Phys. Chem. C* **2015**, *119*, 10427−10438.
(64) Kozuch, S. A Refinement of Everyday Thinking: The Energetic Span Model for Kinetic Assessment of Catalytic Cycles. *Wiley Interdiscip. Rev. Comput. Mol. Sci.* **2012**, *2*, 795−815.
(65) Kozuch, S.; Shaik, S. How to Conceptualize Catalytic Cycles? The Energetic Span Model. *Acc. Chem. Res.* **2011**, *44*, 101−110.
(66) Kozuch, S.; Martin, J. M. L. Turning Over Definitions in Catalytic Cycles. *ACS Catal.* **2012**, *2*, 2787−2794.
(67) Kozuch, S.; Shaik, S. A Combined Kinetic-Quantum Mechanical Model for Assessment of Catalytic Cycles: Application to Cross-Coupling and Heck Reactions. *J. Am. Chem. Soc.* **2006**, *128*, 3355−3365.
(68) Bhan, A.; Nicholas Delgass, W. Propane Aromatization over HZSM-5 and Ga/HZSM-5 Catalysts. *Catal. Rev.: Sci. Eng.* **2008**, *50*, 19−151.
(69) Stull, D.; Westrum, E.; Sinke, G. *The Chemical Thermodynamics of Organic Compounds*; Wiley: New York, 1969; pp 1−865.
(70) Meyers, R. A. *Handbook of Petroleum Refining Processes*, 2nd ed.; McGraw-Hill: New York, 1996; pp 1−848.
(71) Frash, M. V.; Van Santen, R. A. Activation of Small Alkanes in Ga-Exchanged Zeolites: A Quantum Chemical Study of Ethane Dehydrogenation. *J. Phys. Chem. A* **2000**, *104*, 2468−2475.
(72) Computational Chemistry Comparison and Benchmark Data-Base, National Institute of Standards and Technology, http://cccbdb.nist.gov/geometriesx.asp (accessed Jan 1, 2017).
(73) Rodrigues, V. D. O.; Faro, A. C. On Catalyst Activation and Reaction Mechanisms in Propane Aromatization on Ga/HZSM5 Catalysts. *Appl. Catal., A* **2012**, *435−436*, 68−77.
(74) Liu, R.; Zhu, H.; Wu, Z.; Qin, Z.; Fan, W.; Wang, J. Aromatization of Propane over Ga-Modified ZSM-5 Catalysts. *Ranliao Huaxue Xuebao* **2015**, *43*, 961−969.
(75) Pauling, L. The Nature of the Chemical Bond. IV. the Energy of Single Bonds and the Relative Electronegativity of Atoms. *J. Am. Chem. Soc.* **1932**, *54*, 3570−3582.
(76) Janda, A.; Bell, A. T. Effects of Si/Al Ratio on the Distribution of Framework Al and on the Rates of Alkane Monomolecular Cracking and Dehydrogenation in H-MFI. *J. Am. Chem. Soc.* **2013**, *135*, 19193−19207.
(77) Gounder, R.; Iglesia, E. Catalytic Consequences of Spatial Constraints and Acid Site Location for Monomolecular Alkane Activation on Zeolites. *J. Am. Chem. Soc.* **2009**, *131*, 1958−1971.
(78) Gabrienko, A. A.; Arzumanov, S. S.; Toktarev, A. V.; Danilova, I. G.; Prosvirin, I. P.; Kriventsov, V. V.; Zaikovskii, V. I.; Freude, D.; Stepanov, A. G. Different Efficiency of Zn2+and ZnO Species for Methane Activation on Zn-Modified Zeolite. *ACS Catal.* **2017**, *7*, 1818−1830.
(79) Arzumanov, S. S.; Gabrienko, A.; Freude, D.; Stepanov, A. G.; Sun, X.; Zhou, S.; Schlangen, M.; Schwarz, H. Competitive Pathways of Methane Activation on Zn2+-Modified ZSM-5 Zeolite: H/D Hydrogen Exchange with Brønsted Acid Sites versus Dissociative Adsorption to Form Zn-Methyl Species. *Catal. Sci. Technol.* **2016**, *6*, 6381−6388.
(80) Gabrienko, A. A.; Arzumanov, S. S.; Luzgin, M. V.; Stepanov, A. G.; Parmon, V. N. Methane Activation on Zn2+-Exchanged ZSM-5 Zeolites. The Effect of Molecular Oxygen Addition. *J. Phys. Chem. C* **2015**, *119*, 24910−24918.
(81) Luzgin, M. V.; Gabrienko, A. A.; Rogov, V. A.; Toktarev, A. V.; Parmon, V. N.; Stepanov, A. G. The "alkyl" and "carbenium" pathways of Methane Activation on Ga-Modified Zeolite BEA: 13C Solid-State NMR and GC-MS Study of Methane Aromatization in the Presence of Higher Alkane. *J. Phys. Chem. C* **2010**, *114*, 21555−21561.
(82) Sun, Y.; Brown, T. C. Catalytic Cracking, Dehydrogenation, and Aromatization of Isobutane over Ga/HZSM-5 and Zn/HZSM-5 at Low Pressures. *Int. J. Chem. Kinet.* **2002**, *34*, 467−480.
(83) Bondil, M. Master's Thesis, École Polytechnique Fédérale de Lausanne, 2017.
(84) Kumar, A.; Sun, S.-S.; Lees, A. J. *Activation of Unreactive Bonds and Organic Synthesis*; Springer: Berlin, 2010; pp 1−275.
(85) Schreiber, M. W.; Plaisance, C. P.; Baumgärtl, M.; Reuter, K.; Jentys, A.; Bermejo-Deval, R.; Lercher, J. A. Lewis-Brønsted Acid Pairs in Ga/H-ZSM-5 to Catalyze Dehydrogenation of Light Alkanes. *J. Am. Chem. Soc.* **2018**, *140*, 4849.

DOI: 10.1021/acscatal.7b04295
ACS Catal. 2018, 8, 6146−6162